Available online at www.sciencedirect.com

SCIENCE DIRECT®

Earth-Science Reviews 69 (2005) 181–233

EARTH-SCIENCE REVIEWS

www.elsevier.com/locate/earscirev

Quaternary fault kinematics and stress tensors along the southern Caribbean from fault-slip data and focal mechanism solutions

Franck A. Audemard*, Gloria Romero, Herbert Rendon, Victor Cano

Funvisis, Apdo. Postal 76.880, Caracas 1070-A, Venezuela

Received 20 May 2003; accepted 17 August 2004

Abstract

Deformation along the southern Caribbean coast, as confirmed by the compilation of stress tensors derived from fault-plane kinematic indicators (microtectonics) and further supported by focal mechanism solutions herein presented, results from a compressive strike-slip (transpressional senso lato) regime characterized by a NNW–SSE maximum horizontal stress ($\varsigma_H=\varsigma_1$) and/or an ENE–WSW minimum ($\varsigma_h=\varsigma_3$ or ς_2) horizontal stress, which is responsible for present activity and kinematics of six sets of brittle features: east–west right-lateral faults, NW–SE right-lateral faults—synthetic Riedel shears, ENE–WSW to east–west dextral faults—P shears, NNW–SSE normal faults, almost north–south left-lateral faults—antithetic Riedel shears, and ENE–WSW reverse faults—sub-parallel to fold axes and mostly in the subsurface; the latter ones being associated to ENE–WSW-trending folding. In this particular region, the brittle deformation obeys the simple shear model, although not all the deformation can be accounted for it since partitioning is also taking place (regional folding and thrusting is essentially due to the normal-to-structure component of the partitioned maximum horizontal stress). Conversely, the maximum horizontal stress on the Maracaibo block and south of the Oca–Ancón fault progressively turns counter-clockwise to become more east–west-oriented, allowing left- and right-lateral slip along the north–south-striking and NE–SW-striking faults, respectively. The orientation and space variation of this regional stress field in western Venezuela results from the superposition of the two major neighboring interplate maximum horizontal stress orientations (ς_H): roughly east–west-trending stress across the Nazca–South America type-B subduction along the pacific coast of Colombia and NNW–SSE-oriented one across the southern Caribbean boundary zone.

Keywords: Quaternary tectonics; Geodynamics; Stress tensor; Focal mechanism solution; Caribbean; Venezuela

1. Introduction

Northern Venezuela essentially lies in the interaction zone between the South America and Caribbean plates, whereas western Venezuela and northern Colombia show a more complex geodynamic setting

* Corresponding author. Fax: +58 2 257 9977.
E-mail addresses: faudemard@funvisis.org.ve (F.A. Audemard), gromero@funvisis.org.ve (G. Romero), hrendon@funvisis.org.ve (H. Rendon), vcano@funvisis.org.ve (V. Cano).

0012-8252/$ - see front matter © 2004 Elsevier B.V. All rights reserved.
doi:10.1016/j.earscirev.2004.08.001

involving a number of tectonic blocks or microplates (Fig. 1). A wide consensus establishes that the Caribbean plate moves eastward relatively to South America (Bell, 1972; Malfait and Dinkelman, 1972; Jordan, 1975; Pindell and Dewey, 1982; Sykes et al., 1982; Wadge and Burke, 1983; among others), this being strongly supported by recent GPS results lately (Freymueller et al., 1993; Kaniuth et al., 1999; Weber et al., 2001a; Pérez et al., 2001; Trenkamp et al., 2002). But this Caribbean–South America plate boundary—which drives and defines active tectonics along northern Venezuela (from Colombia to Trinidad)—is not of the simple dextral type (Soulas, 1986; Beltrán, 1994) since it is an over 100 km wide active transpressional zone (Audemard, 1993, 1998; Singer and Audemard, 1997; Ysaccis et al., 2000), partly occurring offshore and onshore northern Venezuela. Very important positive relieves within the onshore portion of the plate boundary zone, such as the Coastal and Interior ranges (I, J and Q in Fig. 2), are along the northern and eastern Venezuelan coast. This would seem inconsistent with the Caribbean motion vector in a direction 086°ρ2° with respect to the Central range of Trinidad predicted by Weber et al. (2001a), and N084°ρ2°E with respect to South America (Canoa site) by Pérez et al. (2001) from GPS data, which attest for almost pure wrenching along the plate boundary zone and would instead support slight transtension in eastern Venezuela. This issue shall be discussed in more detail later in this paper. This wide transpressional boundary (in its widest definition, meaning coexistence of strike-slip and compression but not necessarily accommodated jointly on one single structure) extends southwestward into the Mérida Andes (MA in Fig. 1). The plate boundary in western Venezuela is eventually up to

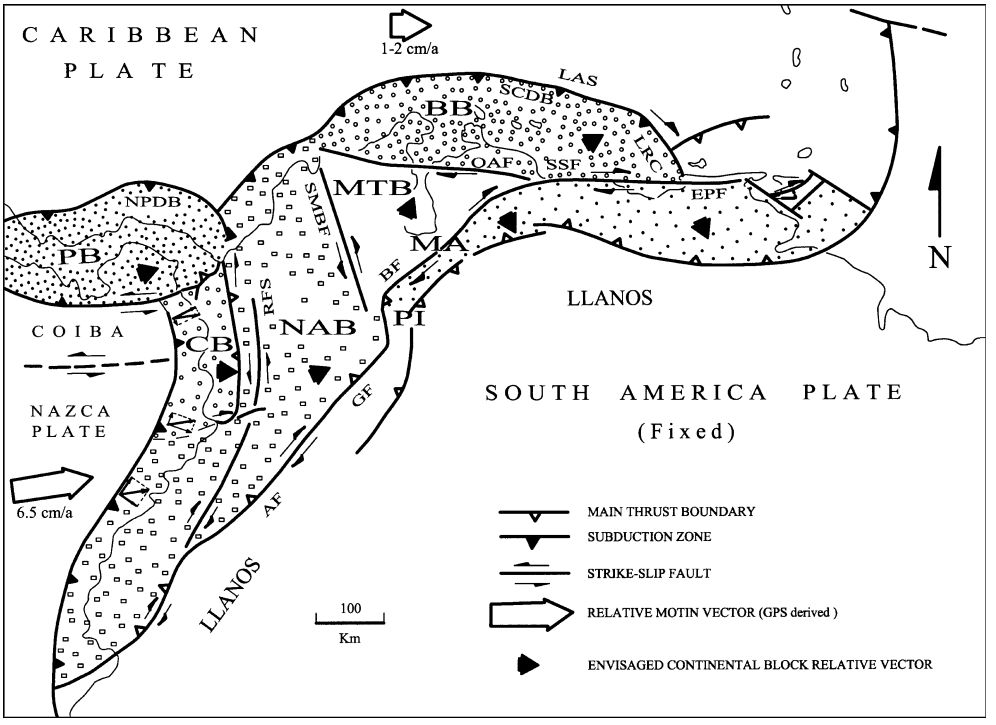

Fig. 1. Simplified general geodynamic setting of the southern Caribbean (modified from Audemard, 2002). Region is subject to a complex block tectonics. Vector decomposition of the convergence vector at the Nazca subduction may explain the along-strike slip change of the Romeral fault system. Equivalence of used acronyms is as follows: Bonaire (BB), Chocó (CB), Maracaibo (MTB), North Andean (NAB) and Panamá (PB) blocks; Mérida Andes (MA) and Pamplona indenter (PI). Some major faults are also reported: Algeciras (AF), Boconó (BF), El Pilar (EPF), Guaicaramo (GF), Romeral (RFS), Santa Marta–Bucaramanga (SMBF), San Sebastián (SSF) and Oca–Ancón (OAF); and other features as well: Leeward Antilles subduction (LAS), Los Roques Canyon (LRC), North Panamá deformation belt (NPDB), and Southern Caribbean deformation belt (SCDB).

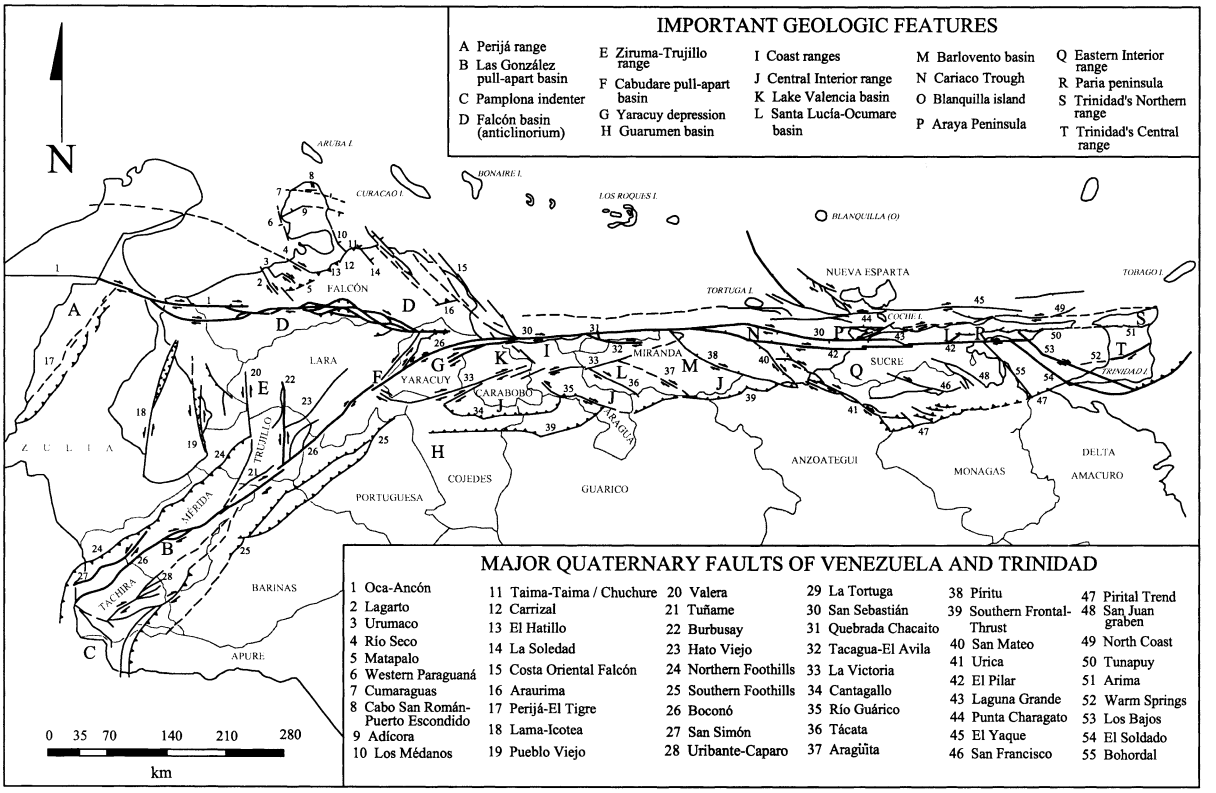

Fig. 2. Schematic map of Quaternary faults of Venezuela (simplified from Audemard et al., 2000). Faults and toponyms used throughout this contribution are identified. Very few localities are only reported in Fig. 3.

600 km wide and comprises a set of discrete tectonic blocks or microplates (Fig. 1), independently moving among the surrounding larger plates (Caribbean, South America and Nazca), among which Maracaibo block stands out for its perfect triangular shape (MTB in Fig. 1). This independent block is bounded by the left-lateral strike-slip Santa Marta–Bucaramanga fault (SMBF) in Colombia and right-lateral strike-slip Boconó fault (BF) in Venezuela and separated on the north from the Bonaire block (BB in Fig. 1) by the right-lateral strike-slip Oca–Ancón fault (OAF). Besides, both Maracaibo and Bonaire blocks are roughly being extruded northward—while the Bonaire block also moves slightly east—and are overriding the Caribbean plate north of the Leeward Antilles islands, where a young south-dipping, amagmatic, flat subduction (LAS) has been forming in recent times (mainly in the last 5 ma). Extrusion of these blocks is induced by the collision of the Panamá arc (PB in Fig. 1) against the Pacific side of northern South America and its later suturing (Audemard, 1993, 1998). Recent results from GPS plate motion studies (Freymueller et al., 1993; Kellogg and Vega, 1995; Kaniuth et al., 1999; Trenkamp et al., 2002), such as the CASA project, confirm this northeastward escape of both blocks, which override the Caribbean plate and generate the Southern Caribbean Deformation Belt (SCDB) north of the Netherlands Leeward Antilles.

The present Caribbean–South American geodynamic configuration results from a transpressive evolution that has occurred throughout the Tertiary and Quaternary, initiated as an oblique type-B subduction (NW-dipping, South American-attached oceanic lithosphere under Caribbean plate island arc). This plate boundary zone later evolved into a long-lasting east-younging oblique-collision (SSE-vergent Caribbean-affinity nappes overriding destroyed-passive-margin-affinity nappes, all overthrusted onto undeformed South America passive margin) and in turn has shifted to a partitioned transpression when

and where collision became unsustainable (for more details refer to Audemard, 1993, 1998). Its latest evolutionary stage is still active in Eastern Venezuela and Trinidad, which recreates the shift from oblique subduction to partitioned oblique collision at present-day of this east-younging oblique convergent margin that has acted diachronically throughout the evolution of this entire northern portion of the plate boundary (Audemard, 2000b). This clearly indicates that, through time, the plate boundary zone has become more of the wrenching type and progressively less compressional, with a major shift in that sense that started at around 17–15 Ma in northwestern Venezuela (Audemard, 1993, 1998). This tectonically complex region in the southeastern Caribbean is undergoing two major geodynamic processes: (a) strain partitioning characterized by NNW–SSE-trending shortening across the entire region from north of La Blanquilla island (O in Fig. 2) to the southernmost active thrust front of the Interior range and right-lateral strike-slip along the main east–west striking El Pilar and NW–SE striking Los Bajos–El Soldado faults, as well as along other minor parallel and/or synthetic Riedel shear faults (Fig. 2); and (b) slab detachment associated with an incipient type-A subduction (e.g., Russo and Speed, 1992; Russo, 1999; responsible for the largest onshore negative Bouguer anomaly of the world, located south of the southern edge of the Interior range). These processes concur with a plate boundary geometry such as the present one, where the El Pilar fault transfers its slip eastward to one of its synthetic Riedel shears (Los Bajos and El Soldado faults), which is acting as a "lithospheric tear fault", thus separating the transpressional boundary on the west from the conventional type-B Lesser Antilles subduction zone on the east. These two distinct seismic domains were originally identified by Pérez and Aggarwal (1981). These different seismicity patterns support contrasting geodynamic contexts (oblique collision and oblique subduction west and east of the Los Bajos–El Soldado fault system, respectively). Recent GPS findings by Weber et al. (2001a) indicate that most of the strike-slip motion of the El Pilar fault is transferred onto the Warm Springs fault system of the Central Range of Trinidad rather than onto a fault south off Trinidad (Fig. 2). This would imply that the Paria gulf is functioning at present as a pull-apart basin bounded by the El Pilar and Warm Springs faults on the north and south, respectively, at a releasing stepover. Both faults exhibit a similar slip rate, in the order of 8–10 mm/year (compare Audemard et al., 2000; Saleh et al., under review). The Warm Springs fault accounts for half of the dextral motion occurring across Trinidad (Saleh et al., under review). So does the El Pilar fault (Audemard et al., 2000), if the relative Caribbean–South America motion is in the order of 20 mm/year in eastern Venezuela, as published by Pérez et al. (2001) and Weber et al. (2001a). However, this crustal deformation does not exclude that a major plate boundary is underlying this region, as portrayed by the instrumental seismicity; conclusion originally drawn by Pérez and Aggarwal (1981) and later confirmed by Sobiesiak et al. (2002).

As in eastern Venezuela, strain partitioning is also a common feature along the rest of the transpressional boundary zone. In the Mérida Andes, strain is nicely partitioned between the right-lateral strike-slip Boconó fault (BF) running slightly oblique along the axis of the chain and thrust faults bounding the chain on both flanks (Audemard and Audemard, 2002). The north-central coastal ranges also exhibit strain partitioning, where dextral slip in the range core is accommodated by both the San Sebastián and La Victoria faults and other minor synthetic Riedel shears, whereas transverse shortening is mainly taken by the relief growth and the frontal thrust faults bounding the chain along its southern edge, such as in the Guarumen basin (Cojedes state; Audemard, 1999b). A mirror thrust fault system may exist on the north but it is under water at present, although the easternmost portion of the Southern Caribbean Deformation Belt and its related type-B subduction (LAS in Fig. 1) should account for some shortening farther north. This configuration both in the Andes and in the eastern Interior range was described by Rod in 1956b and some others, much before the concept of "partitioning" was even formally applied in the mid-1990s.

A large portion of the dextral slip along this complex boundary seems to be presently accommodated by the major right-lateral strike-slip Boconó–San Sebastián–El Pilar–Los Bajos fault system or segments of it (Molnar and Sykes, 1969; Minster and Jordan, 1978; Pérez and Aggarwal, 1981; Stephan, 1982; Schubert, 1980a,b, 1982; Aggarwal, 1983;

Schubert, 1984; Soulas, 1986; Beltrán and Giraldo, 1989; Singer and Audemard, 1997; Audemard et al., 2000; Weber et al., 2001a,b; Pérez et al., 2001). This slip is now known being transferred farther east onto the Warm Springs fault system of central Trinidad (after Weber et al., 2001a's results). It is still matter of debate whether this is either a transcurrent or transform system, depending on the authors and the proposed geodynamic models. Most authors accept or postulate this major right-lateral strike-slip fault system as the plate boundary (e.g., Hess and Maxwell, 1953; Schubert, 1979; Aggarwal, 1983; among many others), whereas few others propose different plate boundary models along this right-lateral strike-slip plate boundary zone: (a) orogenic float type for the Andes (Audemard, 1991a; Jácome, 1994; Audemard and Audemard, 2002) or eastern Venezuela (Ysaccis et al., 2000), thus being flanked by both an A- and B-type subductions; and (b) SE-directed A-subduction or underthrusting under the Mérida Andes (Kellogg and Bonini, 1982; De Toni and Kellogg, 1993; Colletta et al., 1996, 1997). However, the incorporation of the Boconó fault into this major right-lateral strike-slip fault system is a rather recent event, that relates to the northward extrusion of the Maracaibo block, because the former transcurrent boundary used to comprise the east–west-striking Oca–Ancón fault system (OAF) located farther north in northwestern Venezuela (Audemard, 1993, 1998). Therefore, the Oca–Ancón fault system belonged to this major right-lateral strike-slip plate boundary zone along the southern Caribbean from when transpression started at around 17–15 Ma to when essentially ceased or considerably slowed down at around 5–3 Ma. Although the Caribbean with respect to South America is moving at rates between 12 mm/year on the west (geologic slip rate from Nuvel 1-A model) and 18±2 mm/year on the east (GPS-derived slip rate by Weber et al., 2001a,b), the present major strike-slip (Boconó–San Sebastián–El Pilar–Warm Spring faults) boundary slips at ~1 cm/year (Pérez and Aggarwal, 1981; Soulas, 1986; Freymueller et al., 1993; Audemard et al., 2000; Pérez et al., 2001; Weber et al., 2001a,b; Trenkamp et al., 2002), whereas secondary faults at least slip one order of magnitude less faster; as a matter of fact, most of them exhibit slip rates under 0.5 mm/year, except for: Oca–Ancón (2 mm/year, estimated from a paleoseismic assessment performed by Audemard, 1996), Burbusay (δ 3 mm/year), Valera and La Victoria (δ 1 mm/year) faults (for more details, refer to Audemard et al., 2000, and to Fig. 2 for relative location).

We believe that recent GPS results from Pérez et al. (2001) support ongoing transpression in this Caribbean southeastern corner. From these authors' Figs. 1 and 3, four determinant issues can be deduced as to this: (a) the elastic strain across this plate boundary zone affects a region at least 110 km wide; (b) 68% of the 20.5 mm/year right-lateral slip motion measured across most of the plate boundary zone (almost 14 mm/year) is elastically taken by a 30-km-wide fault zone, which includes the El Pilar fault and other subparallel faults located north of it; (c) although subordinate to the right-lateral strike-slip motion, compression is taking place along the plate boundary zone as attested by those vectors located south of the main wrenching system in their Fig. 1, which confirms and supports the earlier collected geologic data through several decades, and compiled to some extent by Audemard et al. (2000); and (d) these slip vectors do not exclude the occurrence of strain partitioning.

This paper presents an updated compilation of stress tensors derived from fault-plane kinematic indicators measured essentially in sedimentary rocks of Plio-Quaternary age along northern continental South America, as well as a few published stress tensors derived from wellbore breakouts, complemented with a compilation of focal mechanism solutions for most important Venezuelan earthquakes of the second half of the past century and beginning of the present one (1957–2003). These datasets are discussed in terms of their interrelation with the regional Quaternary tectonics and their significance with respect to the interactions among the Caribbean, South America and Nazca plates and other involved minor continental blocks of northwestern South America.

2. Quaternary tectonics of Venezuela

Active tectonics in Venezuela at present is driven by tectonic plate and microplate interactions, as explained above. This is the common scenario worldwide. Knowledge about this southern Caribbean plate

boundary zone has much evolved from the original ideas of Hess and Maxwell (1953), when a rather simple dextral wrenching system had been proposed. Over 20 years of neotectonic analysis—which comprises studies in the disciplines of surface geology, geomorphology, microtectonics, seismotectonics and paleoseismology–, combined with data from conventional geologic studies and seismic reflection surveying both onshore and offshore, now give us a more precise view of the complex active geologic setting in Venezuela and surrounds.

Neotectonics for Venezuela, as for everywhere else in the world, is defined as the tectonics resulting from the last and still active stress field. Then, Venezuelan neotectonics refers to the tectonics that takes place in Quaternary times (after Soulas, 1986), implying that tectonic features that either show no evidence of activity during that timeframe or have an orientation not susceptible to be reactivated during the near future under the present stress tensor, are not included in this compilation. The latest version of the neotectonic (Quaternary fault) map depicted in Fig. 3 is the third version of this type of maps (Audemard et al., 2000), after the first version made by Soulas in 1985, and published in 1986 (Soulas, 1986), which was later updated by Beltrán (1993). It differs from previous ones in: (a) new incorporations corresponding to onshore areas studied from the neotectonic viewpoint by Funvisis between 1993 and 1999: the southern frontal thrusts of the Interior range in eastern Venezuela, the southern foothills of the Mérida Andes and a preliminary assessment of the inner active deformation of the triangular block defined by the Oca–Ancón, Boconó and Valera faults; (b) the San Sebastián–El Pilar relay at the Cariaco trough has been reinterpreted, more like the interpretation of Blanco and Giraldo (1992); and (c) although the map is simpler in terms of number of faults (imposed by the aim of the ILP-II-2 project), like near the Colombia–Venezuela border (known as the Pamplona indenter—PI), faults on the map exhibit both their Quaternary kinematics and are discriminated both by age of latest activity and slip rate, which allows easy and quick identification of the major active features. This latest version also includes a report that contains relevant information about each fault and/or fault section (length, attitude, age, sense of slip, slip rate, geomorphic expression, latest activity from geologic data, and so on) and its seismogenic potential (maximum credible earthquake and its recurrence). For more details on these issues, the reader is asked to refer to the accompanying report to the map that is available from the USGS web page.

As mentioned earlier, most of northern and western Venezuela sits on a complex plate boundary zone. Due to this complexity, it is beyond the scope of this paper to discuss all aspects of the Venezuelan neotectonics but to simply portray the main features in order to provide a general outline of the Quaternary tectonics. All names of the active tectonic features used throughout this paper are provided in Fig. 2. Later, the seismotectonics of the region shall be discussed on the basis of focal mechanism solutions and stress tensors derived form fault-slip data.

As imaged in Fig. 3 by Audemard et al. (2000), the following general issues about Venezuela Quaternary tectonics can be put forward.

(1) The Quaternary deformation is not all over the country but strain concentrates along localized stripes or belts (Singer and Audemard, 1997); all of them located in western and northern Venezuela. Most of these mobile belts exhibit high positive relief. So, an important amount of shortening is implicit along this plate boundary, but it does not exclude that some belts show negative relief. The latter features are of more local extent.

(2) The most conspicuous mobile belt is at least 100 km wide and runs over 1200 km in length from the Colombian border near San Cristobal in the southwest into Trinidad in the east. This major belt—which seems to be prolonging from the Eastern Cordillera of Colombia—corresponds to an alignment of mountain chains that comprises from southwest to east: the NE–SW-trending Mérida Andes and the E–W-oriented Coast and Interior ranges both in north-central and northeastern Venezuela. This belt exhibits a first-order dextral fault system that mostly runs along the chain backbone. This system of over 1200 km in length comprises the NE–SW-trending Boconó fault in the Andes section (VE-06 in Fig. 3), and both E–W-striking San Sebastián fault (VE-16 in Fig. 3) in central Venezuela and El Pilar fault (VE-13 in Fig. 3) in eastern Venezuela (Singer and Audemard, 1997). Most of the dextral slip between the Caribbean and South America plates is essentially accommodated by this fault system. In fact, this fault system moves at

Fig. 3. Map of Quaternary faults of Venezuela (after Audemard et al., 2000). Also accessible as a pdf file from the USGS web page in open file reports (ofr-00-0018). Line thickness is proportional to fault slip rate: the thickest indicates >5 mm/year and the thinnest <1 mm/year. Faults with historical or contemporary activity from geologic criteria are in red while Holocene active faults are in yellow. Shown faults, regardless of line color and thickness, have proven Quaternary activity.

about 1 cm/year when most of other faults show slip rates below 1 mm/year (Audemard et al., 2000). Combination of this rather fast slip rate and the significant length of the Boconó–San Sebastián–El Pilar fault system translate into an associated seismicity of moderate frequency and magnitude. This system has been claimed responsible for most large (>7) historical earthquakes that have struck the country since the first ever reported event in 1530; more precisely accounted to some particular segments of this plate boundary (e.g., Rod, 1956a; Cluff and Hansen, 1969; Aggarwal, 1983; Audemard, 1997a,b, 1999c, 2002; Pérez et al., 1997b).

(3) Some secondary mobile zones branch off from the major one. Four of these minor mobile zones are: the E–W-striking dextral Oca–Ancón fault system (VE-01 in Fig. 3) in northwestern Venezuela and three NW–SE trending normal–dextral fault systems respectively located from west to east in eastern Falcón, along the submarine canyon of Los Roques and in the gulf of Paria. The three latter ones exhibit much of negative relief due to the significant normal component involved. Another deformation belt perfectly matches with the NNE–SSW trending Perijá range in westernmost Venezuela, whose crestline defines the border with Colombia.

(4) The major Boconó–San Sebastián–El Pilar fault system displays several structural complexities of kilometric to several-kilometre scale, either in transtension (pull-apart basins such as those of San Juan de Lagunillas—south of Mérida, Cabudare, Cariaco trough, gulf of Paria; among others; refer to Fig. 2 for relative location), or in transpression (Caigüire hills at Cumaná, and Las Manoas and Guarapiche—west and east of the 1997 epicentre, respectively, in Fig. 3; all in Sucre state, in eastern Venezuela and related to the El Pilar fault), but has no complication of regional scale, except for both ends (Singer and Audemard, 1997). On one end, at the Colombia–Venezuela border, the Boconó fault is taken into the Pamplona indenter (as defined by Boinet, 1985). Here, the Boconó fault sharply bends to connect with the N–S-striking Chitagá fault, which shows a strong reverse slip when joining the Boconó fault, but progressively becomes a dominant left-lateral fault towards the south. Farther south, slip is transferred to the NE–SW-trending sinistral Pamplona–Chucarima–Morro Negro fault system (CO-37 in Fig. 3). On the other end, at the Paria gulf and Trinidad, the major right-lateral strike-slip fault system also bends rather sharply, 45° clockwise this time. The fault system splays into several NW–SE-striking offshore faults—among which are the Los Bajos (VE-15 in Fig. 3), El Soldado and Bohordal faults (in Fig. 2)—that exhibit both normal and dextral components. Los Bajos–El Soldado fault system is claimed to link the major transcurrent fault system to the southern tip of the type-B Lesser Antilles subduction; hypothesis that is not necessarily shared by Weber et al. (2001a), who postulate that slip transfer takes place along the Warm Springs fault of the Central Range of Trinidad from repeated GPS measurements. At this eastern tip, the El Pilar fault also shows a splay in the north compartment that branches off towards ENE. This splay, named the Tunapuy fault, exhibits a dominant reverse component with minor dextral slip. Beltrán (1998) proposes that the reverse Tunapuy fault in the Paria peninsula prolongs into the reverse Arima fault of northern Trinidad that bounds the southern foothills of the Northern range of Trinidad (Fig. 2). Weber et al. (2001b) have demonstrated that the Arima fault, based on calcite and quartz geothermometry applied to south-dipping shear bands and cataclastic zones studied along the southern border of the Northern range in Trinidad, is a south-dipping range-bounding normal fault, whose activity as such could not be better resolved than between 12 and 1 Ma. Instead, Saleh et al.'s (under review) results, based on geodetic data (triangulation and GPS data merging), argue for a reverse slip along the Arima fault. So, GPS data seem to confirm the Arima fault slip determined from aerial-photo interpretation based on landforms of Quaternary activity carried out by Beltrán (1998).

(5) Several second-order faults of considerable length diverge obliquely from the major right-lateral strike-slip fault system. Many of them are simply large synthetic Riedel shear faults to the main feature along the direct Caribbean–South America plate interaction in north-central and northeastern Venezuela, such as: Río Guárico (VE-09 in Fig. 3), Tacagua-El Avila (VE-10 in Fig. 3), Tácata (VE-11 in Fig. 3), Píritu (VE-12 in Fig. 3), San Mateo (Jose; VE-14 in Fig. 3), Urica and San Francisco, among several others. In the Andes, the Boconó fault does not image this configuration, although many faults also branch off. Among them deserve mentioning the

north–south-striking sinistral Valera (VE-04 in Fig. 3) and Burbusay faults and the subparallel dextral Caparo fault (SE of San Cristobal; Fig. 2). But this configuration is also present in the Falcón range in association to the Oca–Ancón fault system.

(6) Other fault slips different from the main right-lateral strike-slip fault system—which is also accommodated by synthetic Riedel shears (as mentioned before) and faults sub-parallel to it (e.g., San Simón and Caparo in the Andes, La Victoria in north-central Venezuela and North Coast in eastern Venezuela)—are also present in the mobile belts. Left-lateral strike-slip faults usually trend almost north–south, like the Quebrada Chacaito fault does, but slightly oblique faults to the main dextral system in northeastern Venezuela also exhibit sinistral motion: Punta Charagato fault in the Cubagua island and Laguna Grande fault in the Araya peninsula. Special attention needs to be devoted to these left-lateral strike-slip faults, since their orientation and slip seem atypical with respect to their tectonic setting in northeastern Venezuela. These ENE–WSW-striking faults, in combination with the east–west striking dextral faults, bound wedge-shaped tectonic blocks, whose acute angle points to between ENE and east. Some blocks in this region show a slip vector that slightly diverges to ENE (N084°ρ2°E after Pérez et al., 2001), which matches rather well with the orientation of the bisecting line between both fault trends. This could argue for the occurrence of block expulsions to some extent in this complex south-eastern corner of the Caribbean in order to reduce mass excess. This would give a satisfactory explanation to the apparent transtension postulated by other authors from GPS vectors (e.g., Weber et al., 2001a,b), when transpression is actually the operating mechanism at plate-boundary scale.

(7) Active thrust faults are present along most chain fronts, although they may be blind or hidden behind triangular zones or intracutaneous wedges. They have been detected onshore along the northern edge of the presently inverted Falcón basin (south of Coro), along both Mérida Andes foothills and along the southern front of the Interior range both in central (e.g., Cantagallo overthrust) and eastern (e.g., Pirital and sub-parallel thrusts) Venezuela (Figs. 2 and 3). However, compression is explicitly recorded by chain uplift and build-up, and occasionally by intense folding in sedimentary sequences like in the Falcón basin ("D" in Fig. 2), the eastern Interior range ("Q" in Fig. 2), the Andes foothills, and even in the Neogene–Quaternary foreland sequence of the central Interior range.

(8) Normal faults are also common and widespread within the deformation belts. Tuñame in the Mérida Andes (VE-05 in Fig. 3), Los Médanos (north of Coro), Cabo San Román and Puerto Escondido (north tip of the Paraguaná peninsula in northwestern Venezuela) and Río San Juan graben (in eastern Venezuela) faults are some examples of normal faulting (refer to Fig. 2 for location). Except for the Tuñame fault located in the Andes (Figs. 2 and 3), all other normal faults—which are located in northern Venezuela—strike NNW–SSE. Instead, the normal slip of the Tuñame fault—that roughly strikes ENE–WSW and is located at the convergence of the Valera and Boconó faults—is a consequence of a void effect induced by a bookshelf rotation mechanism produced by simple shear between the Oca–Ancón and Boconó faults.

(9) In western Venezuela, the mobile belt is much wider than in northern Venezuela, reaching up to 600 km in width, and comprises the entire Maracaibo block (MTB) that covers also part of northern Colombia (Audemard, 2000b; Audemard et al., 2000). This block is bounded by the sinistral Bucaramanga fault (SMBF in Fig. 1) on the southwest and the dextral Boconó and Oca–Ancón faults. For other authors, the block is defined on the north by the contact with the flat subduction (LAS in Fig. 1), responsible for the Southern Caribbean Deformation Belt (SCDB) established from seismic tomographic studies by Van der Hilst (1990), rather than by the Oca–Ancón fault system (OAF in Fig. 1). In Venezuelan territory, this block contains two deformation belts with positive relief: the Perijá range and the western part of the Mérida Andes, between which the Maracaibo basin is being squeezed and shortened in NW–SE direction. The Perijá range happens to be the least studied area in terms of active tectonics because of accessibility and personal security.

(10) The triangular Maracaibo block (MTB) shows an intense internal fragmentation where blocks are individualized by north–south to NE–SW trending faults. Most of these faults are essentially left-lateral in slip, with a minor thrust component in many cases, such as from west to east: Icotea, Pueblo Viejo, Valera, Burbusay, among others. This structural and

geometrical configuration may result from a bookshelf rotation mechanism induced by simple shear generated between the dextral Boconó and Oca–Ancón faults (Audemard et al., 1999). But the two faults are not parallel and are at an angle of 45°, which is an atypical configuration that must result in particular complex deformations, as well as switching sense of slip along faults through time.

(11) Fault and fold spatial configuration at regional scale and their kinematics, both deduced from the neotectonic mapping solely, points out that the Northern Falcón basin (northwestern Venezuela) is undergoing a stress tensor characterized by a NNW–SSE to N–S maximum horizontal stress and an ENE–WSW minimum (or intermediate) horizontal stress (Audemard, 1993, 1997b, 2001), thus meaning that the simple shear model associated with strike-slip faulting proposed by Wilcox et al. (1973) applies; although regional folding does not simply result from wrenching, but also from regional compression. Both folding due to wrenching in close association with the Oca–Ancón fault system (transpression s.s.) and to regional compression occur together (transpression s.l.). The neotectonic mapping in this region also allows gathering the active brittle structures in five distinguishable families based on their orientation and kinematics (Audemard, 1993, 1997b; Audemard and Singer, 1996; Figs. 2 and 3): (1) East–West right-lateral faults (Oca–Ancón Fault System—VE-01, Adícora Fault); (2) NW–SE right-lateral faults, synthetic to the east–west faults (Urumaco—VE-02, Río Seco—VE-03, and La Soledad faults); (3) NNW–SSE normal faults (Western Paraguaná, Cabo San Román, Puerto Escondido and Los Médanos faults, all fault-bounding the Paraguaná peninsula); (4) North–South to NNE–SSW left-lateral faults, antithetic to the east–west faults (Carrizal, El Hatillo and other minor faults); and (5) ENE–WSW reverse faults, parallel to folding axis (Araurima, Taima-Taima/Chuchure and Matapalo faults). In terms of slip rate, most Quaternary tectonic features in Northern Falcón are rather slow, showing slip rates generally below 0.4 mm/year, with the exception of the major east–west-trending right-lateral strike-slip Oca–Ancón fault system whose maximum rate in Venezuela is close to 2 mm/year.

(12) The Coast and Interior ranges of central and eastern Venezuela is the only portion of the plate boundary zone to result from rather simple direct interaction between the Caribbean and South America plates. So does northwestern Venezuela (essentially recorded in the Falcón basin, or applicable at larger scale to the Bonaire block bounded between the Leeward Antilles subduction and the Oca–Ancón fault system). Therefore, this region also complies with the Wilcox et al. (1973)'s simple shear model, at least for the brittle tectonics; and partitioning also takes places along this plate boundary segment. Within the Mesozoic metamorphic-dominated SSE-overthrusted nappes of central Venezuela, six families of active tectonic features are distinguishable from their orientation and present kinematics (Figs. 2 and 3): (1) East–West right-lateral faults (San Sebastián, La Tortuga and El Avila faults); (2) NW–SE right-lateral faults, synthetic to the east–west faults (Río Guárico—VE-09, Tácata—VE-11 and Aragüita faults; (3) NW–SE to NNW–SSE normal–dextral to dextral–normal faults (Píritu—VE-12 and Tacagua—VE-10 faults); (4) North–South to NNE–SSW left-lateral faults, antithetic to the east–west faults (Quebrada Chacaito fault); (5) ENE–WSW reverse faults, parallel to folding axis (Nappe fronts, among which the Cantagallo overthrust); and (6) ENE–WSW to E–W dextral faults—P shears (La Victoria fault—VE-08). This is actually the only case of active *P* faulting recognized in the plate boundary zone.

(13) For eastern Venezuela, the configuration of the active structures is as follows (Figs. 2 and 3): (1) East–West right-lateral faults (El Pilar—VE-13, El Yaque and North Coast faults); (2) NW–SE right-lateral faults, synthetic to the east–west faults (San Mateo—VE-14, Urica and San Francisco faults); (3) NW–SE to NNW–SSE normal–dextral to dextral–normal faults (San Juan Graben, Bohordal, Los Bajos and El Soldado—VE-15—faults); (4) ENE–WSW left-lateral faults, which do not obey the simple shear model (Laguna Grande and Punta Charagato faults; issue discussed earlier in this paper); and (5) ENE–WSW reverse faults, parallel to folding axis (frontal thrust of the Interior range, among which the Pirital thrust stands out).

(14) All present deformations along northern Venezuela are to be related to the present oblique convergence vector directed WNW–ESE of the Caribbean plate with respect to South America (e.g., N75°W, after Minster and Jordan, 1978; later confirmed by many others from GPS data, as indicated

earlier). Meanwhile, western Venezuela is undergoing a more complex scenario that shall be described later in this paper. This scenario is even affected by the convergence vector between the Nazca and South America plates that sits much farther south, in Colombian territory.

3. Instrumental seismicity

Seismicity in Venezuela clearly matches geographically with the deformation belts (compare Figs. 3 and 4), and consequently with areas of positive relief (Mérida Andes, Coast and Interior ranges and Perijá, Ziruma–Trujillo and Falcón ranges). Seismicity nationwide is shallow and essentially lies in the first 20 km (Fig. 4A), with the rare exception of certain seismicity deeper than 40 km and mainly intermediate in depth that lies under the continental shelf off northern Falcón and the Zulia (Perijá), Falcón and Lara states, in northwestern Venezuela (Fig. 4B). This seismic activity had been already reported by Van der Hilst (1990); and later seismologically studied in more detail by Malavé and Súarez (1995), Pérez et al. (1997a) and Jaimes et al. (1998). Besides, there are two other regions exhibiting seismicity deeper than 40 km but essentially outside Venezuela (Fig. 4B): (a) the southern tip of the Lesser Antilles subduction under Trinidad and Tobago, the Paria peninsula and the active island arc of the Lesser Antilles and (b) the Bucaramanga nest in Colombia, but near the border with Venezuela. Seismicity of the southern termination of the Antilles subduction has been studied to a certain extent (Pérez and Aggarwal, 1981; Russo et al., 1992; Choy et al., 1998; Sobiesiak et al., 2002, among many others). Those studies have led to establishing the existence of two very distinct seismotectonic provinces that are juxtaposed by the Los Bajos–El Soldado fault system within the Paria gulf. The first province—located SW of the fault system—is characterized by an intracontinental shallow seismicity, whereas the second one perfectly images the NW-sinking intermediate-dip slab of the southern termination of the Lesser Antilles oceanic subduction.

Seismicity in Venezuela, as clearly imaged by Fig. 4, is diffuse and small to moderate in magnitude. This supports the fact that the plate boundary zone is rather wide and tectonic activity is distributed among many active faults within mobile belts (Audemard and Romero, 1993). But this makes reliable seismotectonic associations almost an impossible task (Audemard and Singer, 1997). However, the instrumental seismicity distribution along the major wrenching boundary zone reveals some gaps (Audemard, 2002), from SW to east: (1) along the southwesternmost segment of the Boconó fault, astride Táchira and Mérida states; (2) along the Boconó and San Sebastián faults, between Barquisimeto and west of Choroní (sea town north of Maracay, Aragua state); and (3) along the San Sebastián and El Pilar faults, between north of the Guarenas–Guatire depression (about 20 km east of Caracas) and Cumaná (Sucre state). As verified by Audemard (2002), these present seismic gaps match rather well with the individual fault segments broken during some of the largest most recent historical earthquakes: 1894 in the southern Andes; 1812 in the Yaracuy depression and 1853 (El Pilar splay) and 1900 (San Sebastián splay) along the Cariaco trough.

4. Stress tensors from microtectonic data

We present herein a first compilation and integration of stress tensors derived from geologic (microtectonic) data at national scale, which has been originally collected by Funvisis. In order to ascertain the characterization of the latest and still active tectonic phase, this compilation only integrates stress tensors derived from Plio-Quaternary sedimentary rocks. The data are presented in two different—but complementary—ways: (1) stress tensors are characterized numerically in Table 1. Relevant issues such as location of the microtectonic analysis, performer of the analysis, quality of the data, size of the dataset, age of the deformation or of the disturbed sedimentary sequence are also given; and (2) stress tensors derived from microtectonic data, as well as wellbore data, are displayed in Fig. 5. This compilation map has been fractioned into three parts for a better quality, more legible display (western, central and eastern Venezuela, corresponding to Fig. 5a through c, respectively). These three fraction maps can be easily overlapped and merged in one, if needed. A few stress tensors derived from in-situ borehole data (from natural breakouts or hydraulic fracturing) are also incorporated herein. Scarcity of this type of data is directly related to

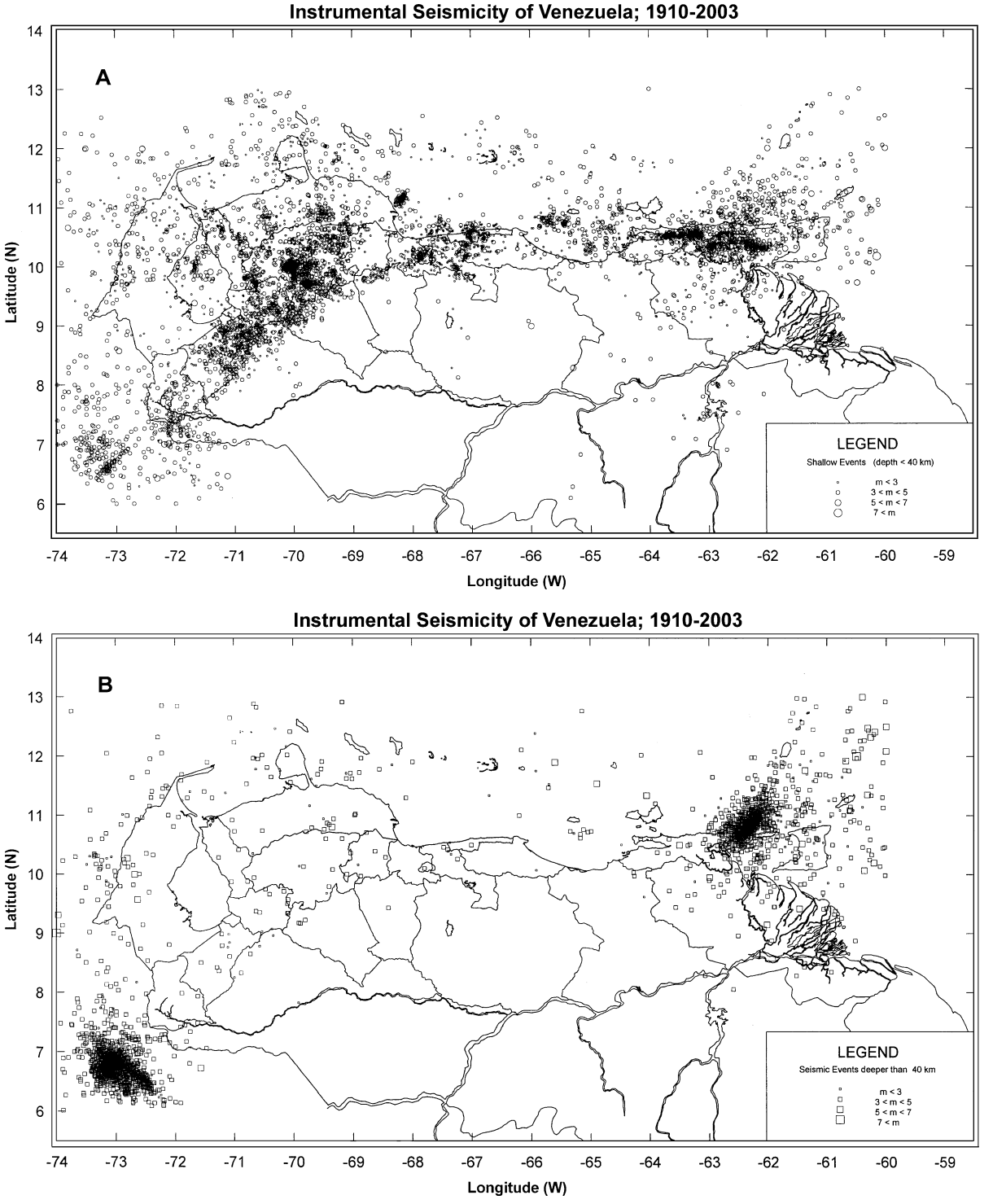

Fig. 4. Instrumental seismicity of Venezuela, between 1910 and 2003 (from Funvisis seismic catalog). Earthquakes are categorized by both magnitude and depth. (A) Events shallower than 40 km; (B) events deeper than 40 km.

Table 1
Compilation of Quaternary stress tensor data obtained by inversion methods relying on fault-plane kinematic indicators; and rarely on disposition of major active tectonic structures (updated and modified from Audemard et al., 1999)

Quaternary stress tensors								
Station no. (ξ)	Locality	σ_H (max)		σ_h (min)		Age	Observations and interpretations	Reference
		Strike	Dip	Strike	Dip			
1	Central-western Falcón	N 117°±12°	Subhor.	N 027°	Subhor.	Pliocene	Determined from regional structure configuration.	Soulas et al., 1987
2	Central-western Falcón	N 160°±06°	Subhor.			Q	Determined from regional structure configuration.	Soulas et al., 1987
3	Central-northern Falcón	N 170°	Subhor.			Q	Originally estimated by Total-CFP. Determined from spatial configuration of regional structures.	Audemard and De Mena, 1985
4	Central-northern Falcón	N 130°–140°	Subhor.			Pliocene	Determined from fractures affecting sedimentary rocks of various ages.	Wozniak and Wozniak, 1979
5	Central-northern Falcón Lat: +11.37°; Long: −69.47°	N 170° to N–S	Subhor.			Q	Established from structural analyses at different scales.	Wozniak and Wozniak, 1979
6	Oca Fault; Hato El Guayabal; (western Falcón) Lat: +10.90°; Long: −71°	N 137°	Subhor. (1°N)	N 054°	Subhor. (4°S)	Holocene	Compressive transcurrent regime. Data from paleoseismic trench. Few measures.	Audemard, 1993
7	Río Seco Fault; near pipelines Lat: +11.37°; Long: −70.13°	N 170°	Subhor. (10°N)	N 077°	Subhor. (16°S)	Q	Excellent microtectonic station. Compressive transcurrent regime.	Audemard, 1993, 1997b; Audemard, 2001; Audemard et al., 1992
8	Falla Río Seco; close to Mitare Lat: +11.30°; Long: −69.98°	N 158°	20°N	N 150°	71°S	Q	Good quality microtectonic dataset. Compressive regime.	Audemard, 1993, 2001; Audemard et al., 1992
9	Urumaco Fault; close to Mamón creek Lat: +11.25°; Long: −70.23°	N 151°E	Subhor. (12°N)	N 064°	Subhor. (12°N)	Q	Excellent microtectonic station. Transcurrent regime.	Audemard, 1993, 1997b; Audemard, 2001; Audemard et al., 1992
10	Punta Sauca (Falcón state) Lat: +11.47° Long: −68.87°	N 122°E	Subhor. (4°N)	N 024°	47°S	Pliocene (?)	Syn-sedimentary to Punta Gavilán fm. deposition. Stress tensor apparently tilted with sequence. Superimposed younger tectonic phase?	Audemard, 1993; Audemard et al., 1992

11	Caujarao (Falcón state) Lat: +11.40° Long: −69.63°	N 350°±21°	Subhor.	Subvertical		Q	Younger than Coro fm. deposition. Transcurrent compressive to compressive regime. Excellent microtectonic station. Shows the progressive northward tilting of the fanglomerate sequence.	Audemard, 1993, 1997b Audemard, 2001; Audemard et al., 1992
12	La Vela anticline, at Puente de Piedra (Falcón state) Lat: +11.52°; Long: −69.42°	N 166°	Subhor. (17°N)	N 022°	69°S	Q	Transcurrent compressive to compressive regime. Good quality microtectonic station, regardless of few measures.	Audemard, 1993, 2001; Audemard et al., 1992; Gallardo, 1985
13	Camare dam (Oca–Ancón fault system) Lat: +10.90°; Long: −70.13°	N 155°	Subhor.	N 075°	Subhor.	Q	In fault gouge material. Good quality microtectonic station, regardless of few measures.	Gallardo, 1985
14	Ziruma–Trujillo range Estimates: Lat: +10.20°; Long: −70.75°	N 160[a]	Subhor.			Post-Miocene	Acute angle between conjugate strike-slip faults: N140°-striking right-lateral, N180°striking left-lateral	Mathieu, 1989
15	Guarumen basin	N 160°	Subhor.			Q	Established normal to thrust faults.	Blin, 1989
16	Yay (Lara state) Lat: +9.78°; Long: −69.63°					Pliocene	Sub-radial extension ($\sigma_{H_{max}} \neq \sigma_1$). σ_1=N 106° 62°W (after counter-tilting sequence, σ_1 becomes vertical)	Giraldo, 1985a,b
17	Quibor–Cubiro road (km 10) Lat: +9.85°; Long: −69.60°	N 110°	Subhor.	N 020°	Subhor.	Q	Transcurrent compressive regime.	Giraldo, 1985a,b
18	San Jerónimo (Lara state) Lat: +9.85°; Long: −69.52°	σ_2: N 70°	Subhor.	N 160°	Subhor.	Q	Localized extension (σ_1 vertical) in probable pull-apart basin at fault divergence between Boconó fault and one of its synthetic Riedel shears (*). σ_2 would be σ_H max	Giraldo, 1985a,b
19	3 km to the NE of Buena Vista (in valley of Turbio river, Lara state) Lat: +9.88°; Long: −69.48°	N 070°	Subhor.			Q	Derived from acute angle between conjugate strike-slip faults (*). Related to the Boconó fault.	Giraldo, 1985a,b

(continued on next page)

Table 1 (*continued*)

Quaternary stress tensors								
Station no. (ξ)	Locality	σ_H (max)		σ_h (min)		Age	Observations and interpretations	Reference
		Strike	Dip	Strike	Dip			
20	El Cerrito, between Buena Vista and Loma El León (valley of Turbio river) Lat: +9.95°; Long: −69.42°					Q	Radial extension (σ_2~σ_3). Excellent microtectonic station: several measures of striations on normal fault planes. Local significance? Related to geometry of the Boconó fault?	Giraldo, 1985a,b
21	Berlín (east side of artificial lake of Dos Cerritos dam, south of El Tocuyo) Lat: +9.67°; Long: −69.92°	N 095°	Subhor.			Q	Transcurrent compressive regime. Related to the dextral Tocuyo fault. Excellent microtectonic station.	Giraldo, 1985a,b
22	Piedras Pintadas; Lake Valencia basin (Carabobo state) Lat: +10.15°; Long: −68.08°	N 115°ρ25°	Subhor.	N 025°ρ25°	Subhor.	Q	North of Tocuyito. Few measures in Lower Pleistocene alluvial deposits.	Audemard et al., 1988, 1995
23	La Pedrera; Lake Valencia basin (Carabobo state) Lat: +10.13°; Long: −68.13°	N 110°ρ40°	Subhor. to interm.			Q	Near water tank north of Tocuyito, in Lower Pleistocene alluvial deposits. Few microtectonic measures.	Audemard et al., 1988, 1995
24	Arpeta; Lake Valencia basin (Carabobo state) Lat: +10.07°; Long: −68.15°	N 010°ρ25°	Subhor. to interm.	N 100°ρ30°	Subhor. to interm.	Q	In gravel pit located to SE of la Lagunita. Few microtectonic measures.	Audemard et al., 1988, 1995
25	Villa de Cura (Aragua state) Lat: +10.05° Long: −67.47°	N 145°E	Subhor.	N 055°	Subhor.	Q	Roadcut 2 km north of Villa de Cura, on road to Cagua. Good datatset in lower Pleistocene alluvial deposits.	Audemard et al., 1988
26	La Puerta (Aragua state) Lat: +9.95°; Long: −67.37°	N 120°E	Subhor.	N 030°	Subhor.	Q?	In gouge of La Puerta fault, on Villa de Cura–San Juan de Los Morros road.Good microtectonic dataset.	Audemard et al., 1988

27	Hacienda La Morita (Aragua state) Lat: +9.93°; Long: −67.07°	N 160°±30°	Subhor.	N 070°±20°	Subhor.	Q	North of the Camatagua dam. Few microtectonic measures.	Audemard et al., 1988
28	North-central litoral	N 140°	Subhor.			Q?	Based on configuration of structures at regional scale.	Fanti et al., 1980
29	Cantinas; Caracas–La Guaira old road (Federal District) Lat: +10.53°; Long: −66.95°	N 143°	Subhor. (23°S)	N 077°	43°S	Q	North of Cantinas oil tanks, associated to the Tacagua–El Avila fault. Stress tensor slightly tilted south; alike to rock foliation (*)	Acosta, 1995, 1997
30	Gallery in south abutment of first viaduct of Caracas–La Guaira highway (Federal District) Lat: +10.53°; Long: −66.97°	N 169°	33°S	N 069°	57°S	Q?	Stress tensor seems tilted south with respect to other tensors in the region. Good microtectonic dataset.	Audemard et al., 1993
31	Santa Lucia–Ocumare del Tuy graben (Miranda state)	NW–SE	Subhor.			Q	From disposition of structures at regional scale; partly confirmed by microtectonic analyses. Synsedimentary tectonic phase to Tuy Formation and younger.	Beck, 1979, 1986
32	Urbanización Industrial Río Tuy (south of Charallave) Lat: +10.22°; Long: −66.87°	N 08°±07°	Subhor. or Subvert.	Sub-vertical		Q	Deformation in Tuy Formation of Plio–Q age. Good microtectonic dataset.	Audemard, 1984, 1985; Loyo, 1986
33	W of Cúa and SW of road junction leading to San Casimiro and Tácata (Miranda state) Lat: +10.17°; Long: −66.90°	N 06°±43°	variable	N 104°±37°	variable	Q	Next to metamorphic–sedimentary faulted contact (Tuy fm.). Very small microtectonic dataset.	Audemard, 1984, 1985; Loyo, 1986

(continued on next page)

Table 1 (*continued*)

Quaternary stress tensors								
Station no. (ξ)	Locality	σ_H (max)		σ_h (min)		Age	Observations and interpretations	Reference
		Strike	Dip	Strike	Dip			
34	Santa Lucía sand pit; east of Sta. Lucía and on left bank of Guaire river (Miranda state) Lat: +10.30°; Long: −66.65°	~N–S	Subhor.	E–W	horizontal	Q	Within Tuy fm.(?), near metamorphic–sedimentary contact. calculated tensor: σ_1: N024°E±12°; σ_3: N114°E±12°; with intermediate dips both, before countertilting actual bedding attitude (N053°W 20°S). Few microtectonic measures.	Audemard, 1984, 1985; Loyo, 1986
35	Puente Pichao–Caracas–Sta. Lucía road Lat: +10.37°; Long: −66.63°	N 174°±30°	Subhor.	N 056°	Subhor.	Q	In the basin-margin conglomerates of the Pichao member. The youngest tectonic phase is established from crosscutting relationship between different striation generations. Excellent microtectonic dataset. In association with La Victoria fault.	Audemard, 1984, 1985; Loyo, 1986
36	W of Cúa; south of Cúa–Tácata road (near poultry farm) Lat: +10.17°; Long: −66.90°	~N–S	variable	E–W		Q	Close to (<250 m) metamorphic–sedimentary contact (in Tuy fm.). North tilted sequence. Very few microtectonic measures.	Audemard, 1984, 1985; Loyo, 1986
37	Arichuna; La Peñita exchanger (NE of Charallave); Lat: +10.28; Long: −66.83	N 158°±07°	Subhor.	N 068°±07°	>56°N	Q	In Tuy Formation sedimentary rocks. Excellent microtectonic dataset.	Audemard, 1984, 1985; Loyo, 1986
38	Sta. Lucía–Turgua road Lat: +10.35°; Long: −66.67°	N 135°ρ25°	Subhor.	N 045°ρ25°	Subhor.	Q	NNW of Santa Lucía, at metamorphic–sedimentary contact (in Siquire fm. sedimentary rocks). Few microtectonic measures.	Audemard, 2000a
39	Santa Lucia–Ocumare del Tuy graben (Miranda state)			NE–SW	Subhor.	Pliocene–lower Pleist.	Extensional tectonic phase affecting the entire basin. 17 microtectonic stations spread over the basin support this phase, that predates the Q compressional phase.	Audemard, 1984, 1985; Loyo, 1986

40	Caracas–La Guaira highway Lat: +10.60°; Long: −67°	N 160°	Subhor.	N 070°	Subhor.	Q?	In metamorphic rocks. Small dataset. Compressive transcurrent regime.	Funvisis, 1984
41	Caracas–La Guaira highway	N 150°	Subhor.	N 060°	Subhor.	Q?	In metamorphic rocks. Extensional transcurrent regime. It is likely that σ_H is more oriented N 170°E (*).	Funvisis, 1984
42	Caracas–La Guaira highway; south bank of Tacagua river Lat: +10.57°; Long: −67.02°	N 150°	Subhor.	N 060°	Subhor.	Q	Near the Tacagua–El Avila fault. In metamorphic rocks. Estimated from acute angle between conjugate strike-slip faults.	Funvisis, 1984
43	Boyacá highway, dirt track to Galipán (El Avila range), Caracas Lat: +10.53°; Long: −66.90°	N 140°	Subhor.	N 050°	Subhor.	Q	Derived from acute angle between conjugate strike-slip faults, in metamorphic rocks; and confirmed by meso-structural analyses. In association with the Tacagua–El Avila fault.	Funvisis, 1984
44	Guarenas–Guatire highway (Guarenas–Guatire basin, Miranda state) Lat: +10.47°; Long: −66.52°	N 155°ρ20°	Subhor.	N 065°	Subhor.	Q	Good dataset of strike-slip faults, in Pliocene sedimentary fill of the Guarenas–Guatire basin.	Funvisis, 1984
45	El Rodeo–Guatire (Miranda state) Lat: +10.45°; Long: −66.48°	N 175°ρ30°	Subhor.	N 085°	Subhor.	Q	Large population of conjugate strike-slip faults. In Pliocene fill of the Guarenas–Guatire basin.	Funvisis, 1984
46	Caruao–La Sabana (North-central litoral) Lat: +10.62°; Long: −66.35°	NW–SE (*)	Subhor.	NE–SW (*)	Subhor.	Q?	In Late Tertiary sedimentary rocks (age spanning from Upper Miocene to Pleistocene, depending on author). Few microtectonic (striated plane) measures. (*) Reassessment by Dihedral method. Original ς_H orientation was N 015°E.	Funvisis, 1984

(continued on next page)

Table 1 (*continued*)

Quaternary stress tensors								
Station no. (ξ)	Locality	σ_H (max)		σ_h (min)		Age	Observations and interpretations	Reference
		Strike	Dip	Strike	Dip			
47	Carenero (Barlovento, Miranda state) Lat: +10.53°; Long: −66.12°	N 110°	Subhor.	N 020°	Subhor.	Q	Small population of strike-slip faults, in sedimentary rocks spanning from Upper Miocene to Pleistocene.	Funvisis, 1984
48	Northern Barlovento basin (Miranda state)			NE–SW (025–034°)	Subhor. (<03°)	Late Miocene–Pliocene	Extensional tectonic phase affecting the entire basin. 2 microtectonic stations (Casupo and Carenero) support this phase, that predates the Q transcurrent phase.	Espínola and Ollarves, 2002
49	Higuerote–Carenero region, Miranda state Lat: +10.50°; Long: −66.15°	320°	Subhor. (09)	053°	16°	Q	Transcurrent regime (R=0.45). Very small dataset.	Espínola and Ollarves, 2002
50	Turupa (Qda. Turupa Grande), Miranda state Lat: +10.44°; Long: −66.24°	N–S	Hor.	E–W	Hor.	Q	Determined from vein arrays in carbonate bed.	Espínola and Ollarves, 2002
51	Los Colorados, Barlovento basin, Miranda state Lat: +10.30°; Long: −66.06°	σ_2: 148	Subhor. (13°)	N 058°	Subhor. (04°)	Q	Faulting in Mamporal formation. Transcurrent-extensional regime (R=0.79) of local significance, related to pull-apart basin at horse-tail splay of the La Victoria fault.	Hernández and Rojas, 2002
52	Tapipa, Barlovento basin, Miranda state Lat: +10.24°; Long: −66.35°	σ_2: 174	Subhor. (10°)	N 265°	Subhor. (05°)	Q	Faulting in Caucagua formation. Transcurrent-extensional regime (R=0.95) of local significance, related to pull-apart basin at horse-tail splay of the La Victoria fault.	Hernández and Rojas, 2002

53	Jose; Petrochemical Complex "José Antonio Anzoátegui" (Anzoátegui state) Lat: +10.06°; Long: −64.83°	N 144°	Subhor. (24°S)	N 020°	Subhor. (23°S)	Q	Large population of striated fault planes in alluvial ramps of Early Pleistocene age. Extensional trans current regime. In association to folds at southern tips of the Píritu and San Mateo (Jose) faults.	Audemard and Arzola, 1995
54	El Yaque (Nueva Esparta state) Lat: +10.93°; Long: −63.95°	N–S	Subhor.	E–W	Subhor.	Q	Derived from tension gashes in Upper Pliocene hydro-thermal travertine deposits.	Beltrán and Giraldo, 1989; Giraldo and Beltrán, 1988
55	Cerro El Diablo; east of Araya, Sucre state Lat: +10.63°; Long: −64.15°	~N–S	Subhor.	E–W	Subhor.	Q	Excellent microtectonic dataset in sediments of Cubagua fm. (Upper Miocene–Lower Pliocene).	Beltrán and Giraldo, 1989; Giraldo and Beltrán, 1988
56	El Obispo; east of Araya, Sucre state Lat: +10.63°; Long: −64.00°	N 163°±11°	Subhor.	N080°		Q	Several measures in sedimentary rocks of Cubagua fm. (Upper Miocene–Lower Pliocene).	Beltrán and Giraldo, 1989; Giraldo and Beltrán, 1988
57	Punta Amarilla; east of Manicuare, Sucre state Lat: +10.58°; Long: −64.20°	N 030°±25°	Subhor.	N 120°±15°	Subhor.	Q	Near Laguna Grande fault. Few striated fault planes in Cubagua fm. rocks. Tensor may only have local significance due to proximity to the fault (*)	Beltrán and Giraldo, 1989; Giraldo and Beltrán, 1988
58	Cumaná Brickyard (NE of International Airport; Cumaná, Sucre state) Lat: +10.47°; Long: −64.15°	N 165°±40°	Subhor.			Q	Near the El Pilar fault. From microfaults in Cubagua fm. rocks.	Beltrán and Giraldo, 1989; Giraldo and Beltrán, 1988
59	Marigüitar, southern coast of Cariaco gulf, Sucre state Lat: +10.45°; Long: −63.95°	N 150°±10°	Subhor.	N 60°E	Subhor.	Q	In Pleistocene fine-grained continental sediments.	Beltrán and Giraldo, 1989; Giraldo and Beltrán, 1988

(continued on next page)

Table 1 (*continued*)

Quaternary stress tensors								
Station no. (ξ)	Locality	σ_H (max)		σ_h (min)		Age	Observations and interpretations	Reference
		Strike	Dip	Strike	Dip			
60	Juan Sánchez village; south of Casanay, Sucre state Lat: +10.48°; Long: −63.31°	N 170°	Subhor.	N080°E	Subhor.	Q	Excellent microtectonic dataset in sedimentary rocks of Cubagua fm. (Upper Miocene–Lower Pliocene).	Beltrán and Giraldo, 1989; Giraldo and Beltrán, 1988
61	Northeastern Venezuela	NNW–SSE (NW–SE to N–S)	Subhor.	NE–SW	Subhor.	Q	Derived from spatial disposition of major structures (folds and faults) and fault kinematics.	Beltrán and Giraldo, 1989; Giraldo and Beltrán, 1988
62	Campoma (heading to Chiguana) Edo. Sucre Lat: +10.51°; Long: −63.61°	N 160°±20°	Subhor.			Q	Derived from orientation of synsedimentary folding axis in Chiguana fm. sedimentary rocks of Pliocene–Lower Pleistocene age.	Mocquet, 1984
63	Villa Frontado; in road to Blascoa, Sucre state Lat: +10.47°; Long: −63.65°	N 015°±30°	variable	N 105°±40°	variable	Q	Few measures in sediments of Villa Frontado fm (Pliocene–Lower Pleistocene). After revision, new σ_H orientation becomes N160°E.	Mocquet, 1984
64	Los Carneros Point; Caribbean coast of Araya Península; Sucre state Lat: +10.65°; Long: −63.71°	N 135°±20°	Subhor. to interm.	N 045°±20°	Subhor. to interm.	Q	In association with Laguna Grande fault	Mocquet, 1984

65	1.5 km to the south of Cariaco; Sucre state Lat: +10.48°; Long: −63.53°	N 140°±40°	Subhor. to interm.			Q	Few measures in sediments of Villa Frontado fm (Pliocene–Lower Pleistocene). Close to El Pilar fault, which may disturb the stress field (*)	Mocquet, 1984
66	Punta de Piedra; eastern Sucre state Lat: +10.54°; Long: −62.43°	σ_2: 267	Subhor. (07°)	174°	22°	Q	Radial extension (R=0.08) of local significance, related to pull-apart basin at step-over between the El Pilar and Warm Springs faults. Microtectonic station of rather good quality. Faulting in Río Salado formation, at northern tip of the Los Bajos fault.	Audemard et al., 2003
67	Río Arriba; eastern Sucre state Lat: +10.63°; Long: −62.40°	147°	11°	241°	19°	Q	Faulting in Río Salado formation. Transcurrent-extensional regime (R=0.70) of local significance, related to pull-apart basin at step-over between the El Pilar and Warm Springs faults. Microtectonic station of low quality due to very small dataset.	Audemard et al., 2003

(ξ) The station no. corresponds to Fig. 4 labelling.
(*) Authors' own interpretation.

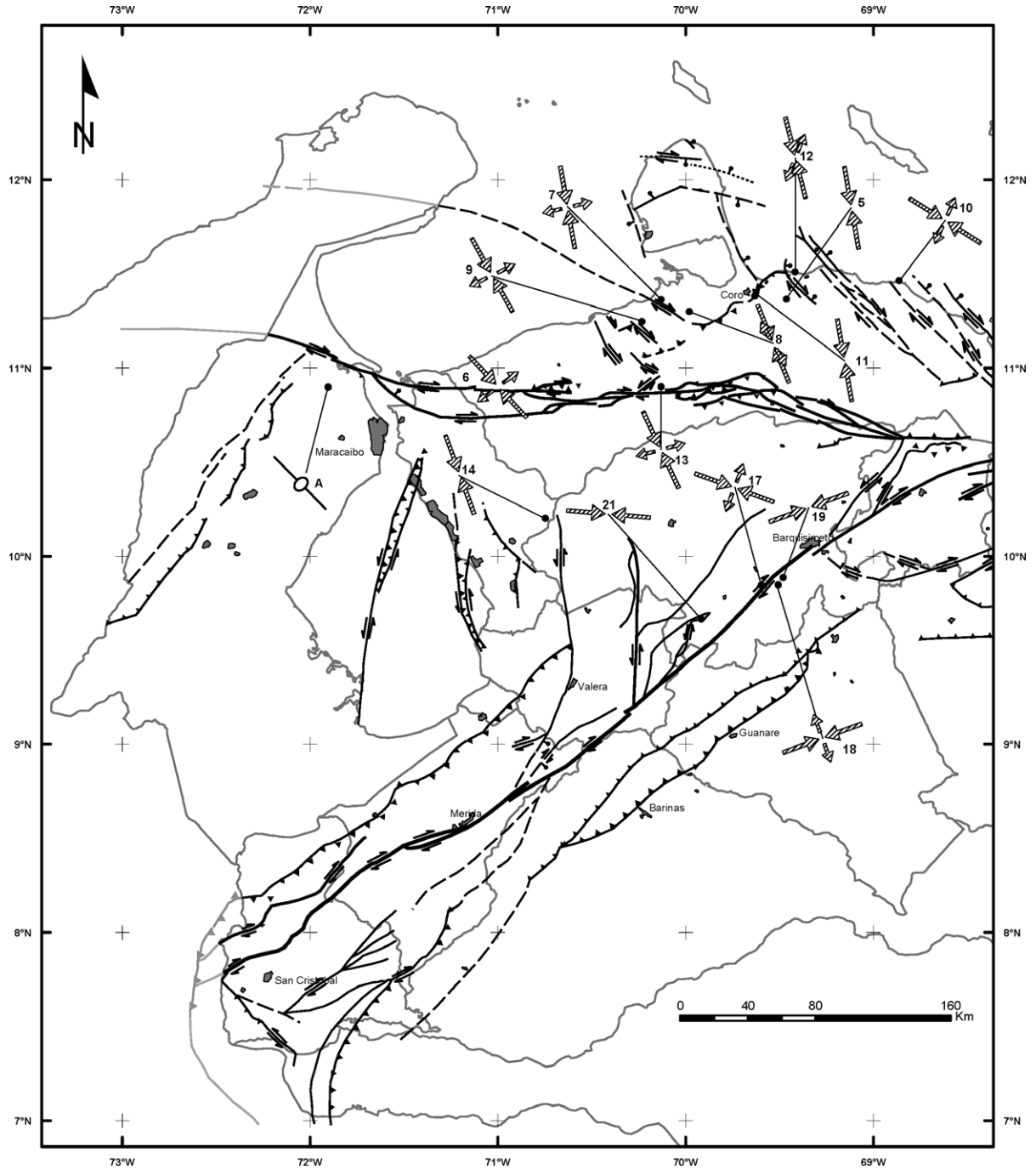

Fig. 5. Map of Plio-Quaternary stress tensors for Venezuela derived from fault-slip data (Table 1; updated and modified from Audemard et al., 1999) and wellbore data (Table 2). Note: non-orthogonal stress axes in plan-view imply that the stress tensor is off the vertical position. Wellbore data (A through D) are represented by either ellipses for breakouts, where ς_H is indicated by the axis, or an open fissure for hydraulic fracturing; or both representations. Stress tensor labelling corresponds to the numbers in Table 1. As to the wellbore data, datapoint A is from Sánchez et al. (1999), datapoints B and C are from Muñoz (2002) and D is from Willson et al. (1999). This map is fractioned regionally in three (a through c): western, central and eastern Venezuela. The tectonic base map corresponds to the one displayed in Figs. 2 and 3 (for toponyms, refer to those figures).

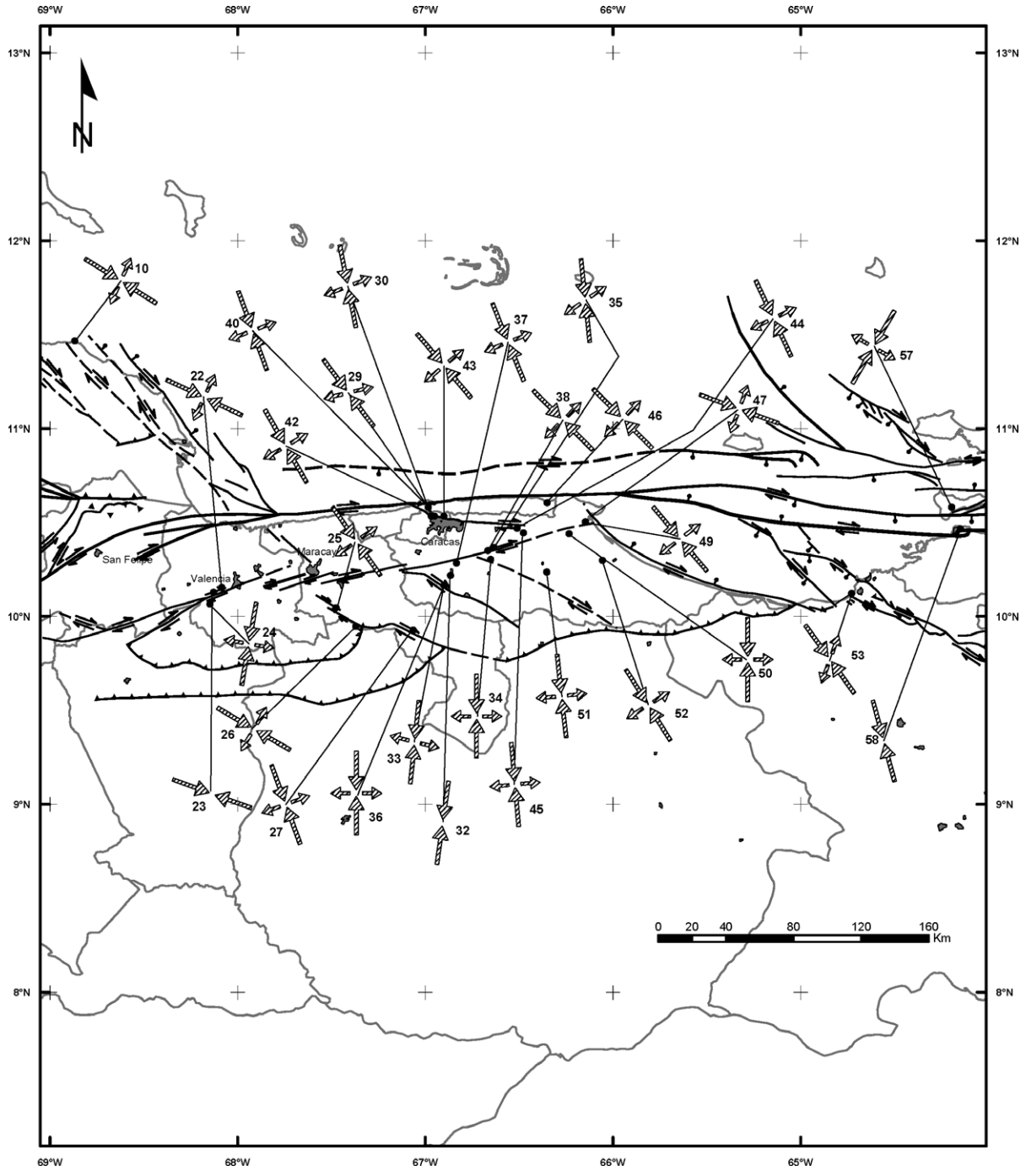

Fig. 5 (*continued*).

confidentiality imposed by the Venezuelan oil-industry. In general, these data are rarely released; and even more rarely published (e.g., Sánchez et al., 1999; Willson et al., 1999; Muñoz, 2002). The same table format as for the Quaternary stress tensors derived from microtectonic data has been used for

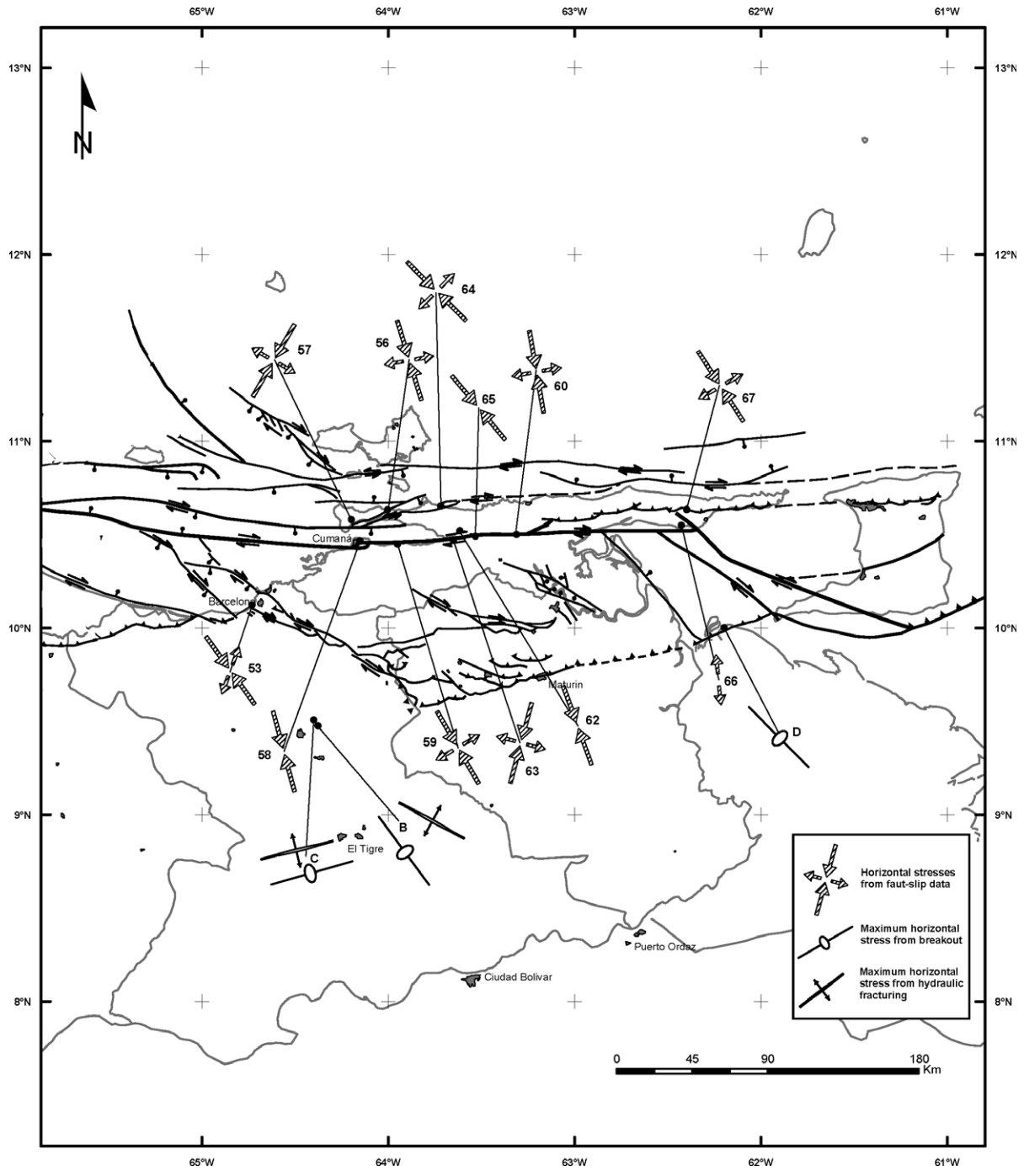

Fig. 5 (*continued*).

those from wellbore data, which are summarized in Table 2. Table labels perfectly correspond to Fig. 5 labelling.

Previously to the present compilation and integration of stress tensors derived from geologic (microtectonic) data at national scale, this type of attempt

Table 2
Compilation of available stress tensors derived from borehole data

Stress tensors from wellbore data						
No.	Locality	ς_H (max)	ς_h (min)	Depth	Observations and interpretations	Reference
1	Mara Oeste oil-field northwestern plain of Maracaibo lake, Zulia state Estimates: Lat: +10.90° Long: −71.90°	N 135°	N 045°			Sánchez et al., 1999
2	Santa Rosa Dome, Area Mayor de Oficina, 10 km NE of Anaco, Anzoátegui state. Estimates: Lat: +9.483° Long: −64.383°	N 135°	N 045°	6800′	Well RG231 located on dome crest In Oficina formation. Breakout orientations: N 045°	Muñoz, 2002
3	Santa Rosa Dome, Area Mayor de Oficina, 10 km NE of Anaco, Anzoátegui state. Estimates: Lat: +9.483° Long: −64.383°	N 140–150°	N 050–060°	9900′	Well RG231 located on dome crest In Merecure formation. Breakout orientations: N 050–060°	Muñoz, 2002
4	Santa Rosa Dome, Area Mayor de Oficina, 10 km NE of Anaco, Anzoátegui state. Estimates: Lat: +9.483° Long: −64.383°	N 130–150° and N 170°	N 040–060° and N 080°	11,000′	Well RG231 located on dome crest In San Juan formation. Breakout orientations: N 040–060° and 080°	Muñoz, 2002
5	Santa Rosa Dome, Area Mayor de Oficina, 10 km NE of Anaco, Anzoátegui state. Estimates: Lat: +9.483° Long: −64.383°	N 145–160°	N 055–070°	12,500′	Well RG231 located on dome crest In San Antonio formation. Breakout orientations: N 055–070°	Muñoz, 2002
6	Santa Rosa Dome, Area Mayor de Oficina, 10 km NE of Anaco, Anzoátegui state. Estimates: Lat: +9.483° Long: −64.383°	N 120° N 145–160°	N 030° N 055–070° N 088°	13,500′	Well RG231 located on dome crest In San Antonio formation, near main thrust fault plane. Breakout orientations: N 030°, N 055–070° and N088°	Muñoz, 2002
7	Santa Rosa Dome, Area Mayor de Oficina, 10 km NE of Anaco, Anzoátegui state. Estimates: Lat: +9.483° Long: −64.383°	N 135° N 175° N 025°	N 045° N 085° N 115°	14,000′ => 15,256′	Well RG231 located on dome crest In Oficina formation, right under the thrust. Breakout orientations: very variable but three predominant modes: N045°, N 085° and N 115°	Muñoz, 2002
8	Santa Rosa Dome, Area Mayor de Oficina, 10 km NE of Anaco, Anzoátegui state. Estimates: Lat: +9.483° Long: −64.383°	N 120–130°	N 030–040°	Not indicated	Well RG231 located on dome crest Hydraulic fractures: N 120–130°	Muñoz, 2002

(continued on next page)

Table 2 (*continued*)

Stress tensors from wellbore data						
No.	Locality	ς_H (max)	ς_h (min)	Depth	Observations and interpretations	Reference
9	Santa Rosa Dome, Area Mayor de Oficina, 10 km NE of Anaco, Anzoátegui state. Estimates: Lat: +9.508° Long: −64.40°	N 070–080°(*)	N 160–170°	10,000′	Well RG229 located on gently dipping northern limb of the so-called dome (highly asymmetric SSE-verging anticline*) In Oficina formation Breakout orientations: N 160–170° (*) This orientation seems atypical in this region. It may be related to moment bending normal faulting close to fold crest. In such a case, that orientation corresponds to ς_h	Muñoz, 2002
10	Santa Rosa Dome, Area Mayor de Oficina, 10 km NE of Anaco, Anzoátegui state. Estimates: Lat: +9.508° Long: −64.40°	N 070–080°(*)	N 160–170°	Not indicated	Well RG229 located on gently dipping northern limb of the so-called dome Hydraulic fractures: N 070–080° (*) That orientation may well correspond to ς_h, if it is related to moment bending normal faulting	Muñoz, 2002
11	Pedernales oil-field, mouth of the Mánamo river, eastern Venezuela. Estimates: Lat: +10.00° Long: −62.20°	N 135°±30°	N 045°±30°	–	Theoretical wellbore breakouts oriented N 045°±30°, since they were not actually measured, but are derived from reported instabilities during drilling operations in this field	Willson et al., 1999

was only carried out at regional scale. Giraldo and Beltrán (1988) for a CONICIT project, later published by Beltrán and Giraldo (1989), integrated this type of data for eastern Venezuela. In the following two subsections, more details are given by separate as to the applied methodology and the present stress regime that is actuating across Venezuela.

4.1. Methodology

A logic sequence of analysis steps is needed to determine the ongoing stress regime from fault-slip (microtectonic) data in a given region. First, the active tectonic framework of the study region has to be known. To achieve this, the active tectonic features of a given region need to be identified and characterized using two complementary and interrelated activities: (1) aerial photo interpretation of landforms diagnostic of Quaternary faulting and folding, at scales ranging between 1:50,000 and 1:25,000. Several reference works—such as those of Vedder and Wallace (1970), Wesson et al. (1975), Slemmons (1977) and Audemard (1999b)—can be used for this sort of landform analyses; and (2) field verification of the interpreted geomorphic evidence of either brittle or ductile tectonic activity, which then leads to the selection of favourable sites exposing Quaternary deformation, primarily of the brittle type. The detail evaluation of these deformed outcrops, usually named microtectonic analysis for simplification purposes, comprises: (a) detailed logging of the outcrop, through which mesoscopic geometric and/or chronologic relationship among tectonic structures—as well as with respect to sedimentary sequence—are established; (b) determination of fault slip using fault-plane kinematic indicators (grouped here under microtectonic data), among which deserve mention: steps, Riedel shears, recrystallizations, stylolitic peaks, slickolites (oblique stylolites, combining slickensides with stylolites), tool marks and/or gypsum fibre growth in some cases, such as those described by Tjia (1971), Mattauer (1973), Proust et al. (1977), Petit et al. (1983),

Hancock and Barka (1987) and Angelier (1994); and (c) measuring of throws and offsets, generally using crosscutting relationships between tectonic structures and planar sedimentary features. Finally, in the case of evaluating the last tectonic regime, to properly apply this evaluation, age constraints on the onset of the present-day tectonic phase are only achieved when the Neogene–Quaternary litho- and chrono-stratigraphy of the study region are well known beforehand.

In Venezuela, Funvisis' personnel, for over 20 years, have calculated all stress tensors derived from sets of striated fault planes, which have remained mostly unpublished. This approach relies on an inversion method, through which the stress tensor is derived from the measured strain. Therefore, the applied method and quality of the resulting tensors through time have been strongly conditioned by the evolution of the methods. In few words, the collected dataset quality is definitely uneven. In the 1980s, the right dihedral method proposed by Angelier and Mechler (1977) was practiced "by hand" using a lower hemisphere Wulff net. Then, differentiating superposed tectonic phases was a rather heavy and time-consuming task with that crude method. Several automated inverse methods were developed almost simultaneously, including the Angelier and Mechler's method which has also been applied later to focal mechanism populations in order to derive a common stress tensor for earthquake populations that spatially cluster (e.g., Choy et al., 1998; Palme et al., 2001). The large majority of these methods were then at an experimental stage and mainly available to university research staff. In the second half of the 1980s, Funvisis applied the method developed by Etchecopar et al. (1981) among many others (Carey, 1976; Fleischmann and Nemcok, 1991; Phan-Trong, 1993), simply due to availability. This lack of availability did not refrain other researchers to propose stress tensors but only relying on the spatial configuration of major tectonic features, such as in the Falcón basin by Audemard and De Mena (1985).

The Etchecopar et al.'s (1981) method, like many others, is based on the Bott's principle (Bott, 1959), which determines the stress tensor by minimizing the deviation between the shear stress and the measured slip on fault surfaces. Consequently, this tensor calculation depends strongly on determining correctly the sense of slip on each fault of a population, which is obtained from the joint observation of several fault plane kinematic indicators listed earlier in this section, that have to necessarily comply with persistency and consistency among them. For instance, Audemard (1993) collected some 400 measures of fault striations on either fault planes or cobble surfaces in northern Falcón to have a robust dataset (stations 6 through 12 in Table 1). Limitations of this particular inversion method were dealt very thoroughly by Ritz (1991).

Since the neotectonic period in Venezuela, as indicated earlier, corresponds roughly to the Quaternary after Soulas (1986), the microtectonic data collection was essentially performed in Plio-Quaternary sedimentary rocks (Table 1), to ensure that the defined stress tensors do correspond to the ongoing tectonic regime. However, few tensors were exceptionally measured in Mesozoic metamorphic rocks, such as in the Caracas surrounds (stations 29, 30 and 40 through 43, in Table 1). Needless to say that these tensors were only included if in agreement with other tensors obtained in the same region from the adjacent Neogene–Quaternary sedimentary fills of the Santa Lucía–Ocumare del Tuy, Barlovento and lake Valencia depressions and along the northern coast of the central Coast range, near Cabo Codera (La Sabana–Chuspa region); all these localities being in the north-central region of Venezuela and less than 150 km away from Caracas (refer to Fig. 2 for relative location). Moreover, some of these microtectonic stations (locality where a population of several striated fault planes is measured, from which a stress tensor—or as many stress tensors as tectonic phases happened—is later derived by an inversion method) were located near tectonic features of confirmed Quaternary activity (for instance, in the Tacagua valley along the Tacagua fault, located WNW of Caracas; Fig. 2). Some tensors, those ones derived from spatial configuration of major faults/folds, are also listed in Table 1 (Appendix 1) but not included in the compilation shown in Fig. 5, because they were not calculated by an inversion method. Except for those tensors (stations 6 through 13, 16 through 21, 29, 30, 48 through 53, 66 and 67) calculated with the Etchecopar et al.'s (1981) method (Giraldo, 1985a,b; Audemard et al., 1992, 1993, 2003; Audemard, 1993; Acosta, 1995; Audemard and Arzola, 1995; Acosta, 1997; Espínola and Ollarves, 2002; Hernández and Rojas, 2002), the rest have been calculated using the right

dihedral method designed by Angelier and Mechler (1977). This latter method is less accurate than that of Etchecopar et al., which is also capable of establishing the qualitative shape of the stress tensor ellipsoid through the value of "*R*". This ratio *R* is defined as $(\sigma_2-\sigma_3)/(\sigma_1-\sigma_3)$. The principal stress in vertical position indicates the dominant tectonic regime but R helps to better define it (refer to Ritz, 1991, for more details).

The stress tensor compilation herein presented gathers 67 entries from microtectonic data and 6 from wellbore data (4 from breakouts and 2 from hydraulic fracturing; refer to Tables 1 and 2 and Fig. 5), of which about only 59 tensors are reliable. Many tensors have been discarded because (1) they result from just a simplistic regional structural interpretation; or (2) some tensors do not reflect the present-day phase (stations 39 and 48 in Table 1), since a younger tectonic phase is superimposed.

4.2. Stress inversion results

Several main results can be drawn from this compilation (Fig. 5a through c).

(1) Northern Venezuela—covering the Falcón basin and the central and eastern Coast and Interior ranges from west to east—is characterized by a Plio-Quaternary stress tensor of rather uniform and constant orientation throughout. The prevailing orientations of this tensor are NW–SE to NNW–SSE (145° to 170°) and NE–SW to ENE–WSW for the maximum horizontal stress (σ_H) and/or minimum horizontal stress (σ_h), respectively. Therefore, there is a good consistency among stress tensors at regional scale. In addition, tensors derived from microtectonic and wellbore data also agree well among them. This geologically derived tensor mostly represents a transcurrent regime (intermediate stress in vertical position). Where the Etchecopar et al.'s method was applied, such as in the Falcón region (upper part of Fig. 5a), the stress regime can be constrained better and is of the compressive transcurrent type (Audemard, 1991b, 1993, 1997b, 2001). Some authors name this tectonic regime as transpressive and refer to the enlarged sense of the term and do not keep its use only for the localized stress changes introduced by strike-slip motion near the wrench fault. This stress tensor is highly oblique to the general east–west trend of the major wrench faults of northern Venezuela (Oca–Ancón, San Sebastián and El Pilar faults). This strong obliquity is responsible for, on one hand, the occurrence of partitioning (right-lateral strike-slip along east–west trending wrench faults and transverse shortening in NNW–SSE direction). Should partitioning be occurring, is it then appropriate to define the tectonic regime as transpressional? On the other hand, it is also responsible for simultaneous left-lateral strike-slip motion on faults that are slightly oblique to the east–west trending dextral faults, as it is the case of the WSW–ENE-striking Punta Charagato and Laguna Grande faults in eastern Venezuela (Figs. 2 and 5c). It is worth mentioning that many microtectonic stations, if not most of them, are located close to or on major active faults. Therefore, it could be thought that they might just have a local significance. However, their consistency throughout the entire boundary zone between the Caribbean and South America plates gives them a more regional meaning.

(2) Since the stress tensor along northern Venezuela from west to east (from northwestern Colombia to Trinidad) is very constant in its orientation, local variations of the stress regime can be clearly identified. Most of these local stress changes coincide with known transtensional geometries, such as stations 16 (Yay depression; Table 1), 18 (transtension at fault divergence; Fig. 5a), 20 (Cabudare pull-apart basin; relative location in Fig. 2), 51 and 52 (Barlovento basin; Table 1 and Fig. 5b) and 67 (transtensional horse-tail splay at northern tip of Los Bajos fault; Table 1 and Fig. 5c). Occasionally, local variations occur at transpressional geometries (such as station 6 on the Oca fault at Hato El Guayabal; Table 1 and Fig 5a); also in association with bending-moment faulting (normal faulting at anticline crests during buckling; e.g., stations 53 at Jose Petrochemical complex and 66 at Punta de Piedras near Güiria; Table 1 and Fig. 5c). These changes are easily identifiable because the stress tensor orientation remains essentially constant but their principal stress magnitudes vary (stress tensor permutation, where maximum and intermediate stresses may interchange positions).

(3) At an even more local scale, detail microtectonic studies and the subsequent stress tensor determination by an inverse method may allow to reveal, for instance, the occurrence of block rotation

(i.e., between the two strands of the Río Seco fault in northern Falcón; refer to Audemard, 2001) or progressive tectonic tilting (i.e., Guadalupe–Chuchure thrust at the Coro Formation stratotype locality—south of Coro, Falcón state; refer to Audemard, 2001). However, some structures may not definitively be related to the regional stress field and respond to local perturbations of the stress field, such as the folding at Punta Macolla, at the convergence of the Western Paraguaná and Cumaraguas faults, in the Paraguaná peninsula (Audemard, 1993). These particular cases are dealt in detail in the cited references, but are omitted from this compilation because of their very local significance, which is not the aim of this current compilation.

(4) The stress tensor calculated by either the Etchecopar et al.'s (1981) automated method or the right dihedral method of Angelier and Mechler (1977) well represents the stress field for the present-day kinematics of seven major families of active faults along northern Venezuela: (a) east–west right-lateral faults; (b) NW–SE right-lateral faults, synthetic to the east–west faults; (c) NNW–SSE normal faults; (d) NW–SE to NNW–SSE normal–dextral to dextral–normal faults; (e) North–South to NNE–SSW left-lateral faults, antithetic to the east–west faults; (f) ENE–WSW to east–west right-lateral faults—P shears; and (g) ENE–WSW reverse faults, paralleling folding axis, which is also active. Spatial configuration of these brittle tectonic structures indicates that the region is undergoing a transpressional s.l. (compressive-transcurrent) regime that complies with the simple shear model proposed by Wilcox et al. (1973). Therefore, this regional configuration is related to the slightly oblique convergence between the Caribbean and South America plate in the west—and almost perfect wrenching in eastern Venezuela with some "apparent" transtension (Pérez et al., 2001; Weber et al., 2001a,b), that is directly responsible for east–west trending dextral wrenching along northern Venezuela. In northeastern Venezuela, the apparent inconsistency between the GPS derived slip vectors from both Pérez et al. (2001) and Weber et al. (2001a), which would seem to support some transtension north of the El Pilar fault, and the stress tensors herein presented (stations 54 through 61 in Table 1), which seem to support a regionally coherent transpression, can be resolved if microblock extrusions north of the El Pilar fault were occurring. In addition, this would, not only explain the slip vector direction of N84°ρ2°E calculated north of the El Pilar fault, but also the sinistral motion along the ENE–WSW-striking Punta Charagato and Laguna Grande faults. On the other hand, in the particular case of northwestern Venezuela, this process is accentuated by the convergence between the Bonaire block (BB) and the Caribbean plate along the rather flat Southern Caribbean subduction located offshore the Netherland Antilles islands (LAS), which is in turn driven by the NNE-directed extrusion common to the Maracaibo and Bonaire blocks. Consequently, it can be stated that there is a good accordance between stress tensors derived from microtectonic data and large-scale neotectonic structures.

(5) σ_H in the northern Mérida Andes (Lara state), when nearing the Boconó fault, tends to become east–west oriented, which allows the ongoing simultaneous functioning of the NE–SW-striking dextral (e.g., Boconó, Caparo, San Simón) faults, the equally trending thrust faults along both Mérida Andes foothills and the north–south striking sinistral faults (e.g., Valera and Burbusay, among several others; Figs. 2 and 5a).

(6) Therefore, the stress field on the Maracaibo block (MTB) and south of the Oca–Ancón fault progressively turns counterclockwise from a NNW–SSE trend in the north (Beltrán and Giraldo, 1989; Audemard, 2001; this paper) to east–west oriented to the south (Audemard et al., 1999; Fig. 5a). The stress field in this region then resembles like a folding fan with vertex pointing to the SE (Audemard and Audemard, 2002). The orientation of this regional stress field in western Venezuela results from the superposition of the two major neighbouring interplate maximum horizontal stress orientations (ς_H): roughly east–west trending stress across the Nazca–South America type-B subduction along the pacific coast of Colombia and NNW–SSE oriented one across the Caribbean southern boundary (Audemard, 2000b; Fig. 1). Therefore, the Maracaibo block is simultaneously being shortened along the NW–SE direction (expressed by the vertical growth of the Santa Marta block and Perijá and Mérida ranges) and roughly extruded north to NNE (Audemard, 1993, 1998, 2000b; Audemard and Audemard, 2002).

5. Focal mechanisms

Previous focal mechanism solution compilations in Venezuela include local coverage (Giraldo and Beltrán, 1988; Beltrán and Giraldo, 1989; Kozuch, 1995; Choy et al., 1998), and more regional or nationwide coverage (Molnar and Sykes, 1969; Dewey, 1972; Kafka and Weidner, 1981; Pennington, 1981; Cisternas and Gaulon, 1984; Tovar, 1989; Romero, 1994). Most frequent are solutions for single earthquakes (e.g., Rial, 1978; Badell, 1981; Giraldo, 1985b; Suárez and Nabelek, 1990; Ramos and Mendoza, 1993; Rodríguez, 1995; Acosta et al., 1996; Funvisis et al., 1997; Choy, 1998; Pérez, 1998; Audemard, 1999a) or a group of earthquakes in given regions (Marín, 1982; Lozano, 1984; Mendoza, 1989; Bach, 1991; Bach et al., 1992; Malavé, 1992; Russo et al., 1992; CEE-Intevep, 1993; Romero, 1993; Malavé and Súarez, 1995; Valera, 1995) or composite focal mechanisms of rather small magnitude clustered earthquakes (Laffaille, 1981; Pérez and Aggarwal, 1981; Ramos and Mendoza, 1991; Audemard and Romero, 1993; Pérez et al., 1997a,b; Jaimes et al., 1998). Cisternas and Gaulon (1984) have made the first compilation of the entire southern Caribbean region. However, the most thorough focal mechanism compilations for Venezuela prior to the present one are those of Tovar (1989) and Romero (1994); both in unpublished Funvisis reports. The latter compilation forms the core of that we are presenting herein.

5.1. Methods

The present compilation gathers 125 focal mechanism solutions proposed for 114 (single or composite) events (Table 3 and Fig. 6). This difference in number resides in that some earthquakes have occasionally been interpreted as multi-focal events (Caracas 1967—label 09 through 12 in Table 3 and Fig. 6—and Boca de Tocuyo 1989—label 71 through 75 in Table 3 and Fig. 6). On the contrary, two alternate solutions have rarely been proposed for single events (Curarigua August–September 1991—pairs labelled 82–83, 85–86 and 88–89 in Table 3 and Fig. 6—and Los Arangues December 29, 1995—labels 93 and 94 in Table 3 and Fig. 6—earthquakes), which are both compatible with known neighbouring fault kinematics and stress tensor derived from geologic data. For several events, it is worth mentioning that a choice of one solution among many proposed by different authors had to be made, taking into account which would fit best both attitude (strike and dip) and slip of the potentially causative fault. Due to space limitations, we ask the reader to refer to appendix in Audemard et al. (1999; available from the author) for more details on this selection.

This compilation also includes 27 new solutions for earthquakes of small magnitude (<5 mb), recorded by the new Venezuelan seismological network in the last couple of years (solutions labelled 99 through 125 in Table 3), added to the first Audemard et al.'s (1999) compilation. This has been possible because the array has been upgraded (enlarged and modernized) and has 28 new three-component broadband stations installed throughout the country as of April 2003. On the contrary, the present compilation shown in Fig. 6a through c does not incorporate 20 published focal mechanism solutions of small earthquakes, recorded during two microseismicity surveys carried out in western Venezuela (Bach, 1991; Bach et al., 1992; CEE-INTEVEP, 1993), and also in eastern Venezuela in 1990 (CEE-INTEVEP, 1993), by a Comunidad Económica Europea-INTEVEP multidisciplinary task group. Neither the *P* arrivals nor the tension (*T*) and pressure (*P*) axis orientations nor the nodal plane attitudes of those solutions were available. All these data would have allowed the exact reconstruction of the focal mechanisms. Moreover, this information is essential to any reliability assessment or quality control. Some slight picking was performed among the proposed focal solutions by the CEE-INTEVEP group (Fig. 7). The discarded focal mechanisms were originally built as composite solutions and the event gathering for their construction did not follow either any tectonic criteria or time and space clustering. Nevertheless, *P* and *T* axes from focal mechanisms proposed for small earthquakes recorded during that northwestern Venezuela campaign (labelled as 2 in Fig. 7) coincide well with those of Fig. 6.

5.2. Focal mechanism results

Similarly to the stress tensors derived from geologic data, these focal mechanism solutions exhibit good

Table 3
Focal mechanism solutions for Venezuelan earthquakes spanning from 1957 through 2003 (updated and modified from Audemard et al., 1999)

Date (yy/mm/dd)	Latitude (deg)	Longitude (deg)	Focal depth (km)	Magnitude (mb)	Nodal plane A			Nodal plane B			*T* axis		*P* axis		Fig. 5 label no.	Reference
					AZI	DIP	RAKE	AZI	DIP	RAKE	AZI	DIP	AZI	DIP		
57/10/02	10.94	−62.80	60		261	90	180	351	90	0	36	0	126	0	1	Molnar and Sykes, 1969
57/10/02	10.88	−62.90	10	5.5	47	86	135	313	45.14	174.4	171	26.7	280.3	33.2	2	Russo et al., 1992
57/10/04	10.86	−62.77	6	6.7	75	45	41	196	62.4	127	59.8	60.6	316.4	7.4	3	Russo et al., 1992
57/10/06	10.88	−62.68	10		132	44	−90	312	46	−90	42	1	222	89	4	Russo et al., 1992
57/12/25	10.46	−62.55	22	5.8	215	87	100.3	321	10.8	16.3	135.7	47	305	41.1	5	Russo et al., 1992
63/07/14	10.44	−62.74	20		90	63	−123.6	214	42.1	−42.6	216.7	0.9	307.5	41.1	6	Molnar and Sykes, 1969
65/07/19	9.25	−70.44	20.0	5.2	55	90	180	145	90	0.0	190	0.0	280	0.0	7	Dewey, 1972 (in Pennington, 1981)
66/05/14	10.38	−63.05	37		274	71	−173.9	182	84.2	−19.1	229.4	−19.1	136.5	17.5	8	Molnar and Sykes, 1969
67/01/04	10.70	−62.05	74		89	52	−136.8	329	57.4	−47	38.1	3.1	295.7	54.7	9	Molnar and Sykes, 1969
67/07/30	10.60	−67.30	14.0	6.5	261	85	180	351	90	5.0	216.1	3.5	125.9	3.5	10	Suárez and Nabelek, 1990[a]
67/07/30	10.70	−66.95	14.1	6.5	265	69	−177.2	174	87.4	−21	221.4	12.8	127.5	16.6	11	Suárez and Nabelek, 1990[a]
67/07/30	10.18	−66.76	7.7	6.5	50	81	173.6	141	83.7	9.1	5.7	10.8	275.3	1.9	12	Suárez and Nabelek, 1990[a]
67/07/30	10.95	−66.88	21.0	6.5	276	59	128.4	39	47.8	44	239.9	57	339.8	6.4	13	Suárez and Nabelek, 1990[a]
67/12/21	7.00	−72.00	29.0	4.0	138	76	0.0	48	90	166	2.1	9.8	93.9	9.8	14	Dewey, 1972 (in Pennington, 1981)
68/03/12	13.15	−72.30	58	5.3	64	28	90	244	62	90	154	73	334	17	15	Pérez et al., 1997a[a]
68/05/13	9.06	−71.10	29.0	4.9	228	60	130.9	348	49.1	41.4	191.3	54.7	290.2	6.3	16	Dewey, 1972 (in Pennington, 1981)
68/09/20	10.76	−62.70	103.0	6.2	226	15	66.7	70	76.2	96	348.2	58.3	155	31	17	Pérez and Aggarwal, 1981[a]
68/11/17	9.60	−72.60	150.0	5.8	149	8	179	240	89.9	82	142.1	44.6	337.9	44.3	18	Malavé and Súarez, 1995
69/10/20	10.90	−72.40	36.0	5.7	47	50	−52.4	170	65	−136.6	270	9	23	49.0	19	Pennington, 1981
69/10/20	10.87	−72.49	36.0	5.7	2.9	72.3	0.0	92.9	90	−162.3	226.5	12.4	319.3	12.4	20	Malavé, 1992
70/01/27	7.49	−72.09	31	5.6	240	60	−143.9	130	59.4	−35.5	4.9	0.4	95.3	45.6	21	Kafka and Weidner, 1981
70/05/19	10.90	−68.90	15.0	5.1	5	70	−38.1	110	54.6	−155.2	60.6	9.7	322.2	40.7	22	Dewey, 1972 (in Audemard and Romero, 1993)[b]
70/12/14	9.90	−72.68	158.0	5.1	159	14	−122.2	12.0	78.2	−82.4	95.6	32.8	291.6	56.2	23	Malavé, 1997
73/07/08	6.80	−73.00	156.0	5.4	44	64	154.1	146	66.9	28.5	5.8	36	274.5	1.9	24	Pennington, 1981
74/06/12	10.61	−63.47	0.0	5.7	213	70	−31.9	315	60.3	−156.8	265.8	6.3	171.2	36.3	25	Rial, 1978 (in Perez and Aggarwal, 1981)[a]
75/03/05	9.13	−69.87	25	5.6	210	50	56.4	76	50	123.4	52.6	64.9	143.1	0.2	26	Laffaille, 1981 (in Giraldo, 1985b)[a]
75/04/05	10.10	−69.60	36.0	5.5	112	80	168.6	204	78.8	10.2	67.9	15.1	158.1	0.8	27	Molnar and Sykes, 1969 (in Pennington, 1981)
75/04/05	9.56	−69.52	2.0	5.5	294	68	0.0	204	90.0	158	156.8	15.4	251.2	15.4	28	Marín, 1982
77/10/04	10.16	−61.99	21	5.1	273	52	−161	171	75.1	−39.6	226.7	14.7	124.8	38.1	29	CMT

(continued on next page)

Table 3 (*continued*)

Date (yy/mm/dd)	Latitude (deg)	Longitude (deg)	Focal depth (km)	Magnitude (mb)	Nodal plane A			Nodal plane B			*T* axis		*P* axis		Fig. 5 label no.	Reference
					AZI	DIP	RAKE	AZI	DIP	RAKE	AZI	DIP	AZI	DIP		
77/12/11	9.56	−69.52	2.0	5.5	70	65	139.3	180	53.7	31.6	30.2	45.8	127.3	6.9	30	Marín, 1982[b]
79/05/05	9.09	−71.56	22	5.6	119	53	5	26	86	142.9	335.8	28.3	78.5	22.1	31	CMT
79/06/C[c]	10.45	−63.60	1.5		177	85	−11.3	268	78.7	−174.9	222.9	4	132	11.5	32	Pérez and Aggarwal, 1981[b]
79/06/C[c]	10.40	−63.60	1.5		337	75	−161.3	242	72	−15.8	109.1	2	200	23.7	33	Pérez and Aggarwal, 1981[a]
79/07/C[c]	10.50	−63.25	1.5		250	85	−141.3	156	51.4	−6.4	16.6	22.3	120.4	30.2	34	Pérez and Aggarwal, 1981[a]
79/07/C[c]	10.45	−63.17	1.0		58	10	180	148	90	80	48.1	44.1	247.9	44.1	35	Pérez and Aggarwal, 1981[a]
80/01/02/C[c]	8.71	−71.08			29	65	103.2	180	28.1	63.9	323.7	67.3	109.2	19	36	Laffaille, 1981[b]
80/01/02/C[c]	8.66	−71.03			221	30	−106.6	60	61.4	−80.6	143.1	15.9	351.9	72	37	Laffaille, 1981[b]
80/11/26	7.96	−72.62	40	5.2	57	64	170.9	151	81.9	26.3	17	24.2	281.4	12.1	38	CMT
82/05/10	10.50	−62.56	79.8	5.3	204	9	−4	298	89.4	−99	36.8	43.7	199	44.9	39	CMT
82/07/04	7.65	−72.19	53.5	5.5	136	66	4.9	44	85.5	155.9	357.4	20.1	92.4	13.4	40	ISC
83/03/08	10.89	−62.03	85.0	5.9	260	7	119.8	50.0	83.9	86.5	316.1	51.0	143.2	38.8	41	ISC
83/04/11	10.08	−62.61	19.2	6	3	43	−57.6	142	54.9	−116.6	250.6	6.3	356.1	61.5	42	CMT
84/C[c]	8.40	−70.90	20	4	45	44	77.6	242	47.3	101.7	222.9	81.3	323.7	1.7	43	Pérez et al., 1997a
84/02/11	12.08	−60.00	39.1	5.3	348	53	−142.2	233	61	−43.6	292	4	195.5	50.5	44	ISC
84/06/14	10.05	−69.78	18	5.2	340	65	−11.7	75	79.4	−154.5	205.4	9.7	300	25.4	45	CMT
84/08/20	10.62	−62.53	21.8	5.1	80	71	165	175	75	19.6	38.3	23.8	306.8	3.3	46	CMT
84/10/05	11.34	−60.25	41.2	4.4	172	57	−150.7	65	65.8	−36.7	120	5.0	25	43	47	ISC
85/87/90C[c]	9.90	−68.70	15	3− 3.9	168	84	0	78	90	174	32	4.2	123.2	4.2	48	Pérez et al., 1997b
85/87/94C[c]	10.7	−67.00	15	3− 3.9	355	60	0	85	90	−150	215.9	20.7	314.1	20.7	49	Pérez et al., 1997b
85/11/28	11.76	−61.36	49.0	5.2	201	27	123.9	344	68	74.1	227	64	86	21	50	ISC
86/C[c]	10.2	−67.00	15	3.0− 5.8	48	65	−7.1	141	83.6	−25.2	272	12.7	7.3	22.2	51	Pérez et al., 1997b
86/C[c]	9.5	−69.20	20	3.0− 4.0	315	60	0	225	90	150	175.9	20.7	274.1	20.7	52	Pérez et al., 1997b
86/C[c]	9.2	−69.90	20	4.0	190	40	52.5	55	59.3	117	13.3	64.5	125.9	10.4	53	Pérez et al., 1997a
88/89/90C[c]	10.3	−67.00	15	3.0− 4.0	39	75	−31.5	138	59.7	−162.6	91.2	10	351.8	32.7	54	Pérez et al., 1997b
86/06/11	10.7	−62.93	20	6.0	97	52	−159.4	354	73.9	−39.8	50	13.9	308.4	39.1	55	CMT
86/07/18	10.80	−69.35	15.0	5.6	64	41	106.2	223	51	76.4	78	78	323	5	56	ISC
86/07/18C[c]	10.80	−69.36	44.9	5.6	204	85	21.8	112	678.3	174.6	70.1	78.9	336.1	11.6	57	Audemard and Romero, 1993
86/09/12C[c]	11.04	−69.44	8.2	4.4	65	53	144.8	178	62.6	42.7	36.1	48.7	299.5	5.7	58	Audemard and Romero, 1993
87/06/01	12.24	−61.54	156	4.0	62	36	177.5	154	89	54	33	36	274	34	59	ISC
88/C[c]	10.30	−69.80	20	4.0	325	55	180	55	90	145	184	24	286	24	60	Pérez et al., 1997a
88/03/10	10.16	−60.13	54	7.0	256	38	−67.3	48	56	−106.8	150	9.0	274	73	61	ISC
88/0311	10.06	−60.32	47	4.5	213	38	−131.2	81	63	−62.8	152	14	35	62	62	ISC
88/03/12	10.19	−60.20	33	5.3	42	31	−132.6	269	68	−67.9	343	20	213	61	63	ISC

88/03/16	9.72	−60.47	55	5.2	40	45	−118.1	257	51	−64.8	330	3	230	70	64	ISC
88/03/25	10.04	−60.26	56	4.9	16	63	−173.4	283	85	−27.2	333	15	236	23	65	ISC
88/04/12	10.35	−63.00	53.9	5.5	66	45	136.4	190	60.8	54.1	49.2	57.7	301.8	8.9	66	CMT
88/06/24	10.28	−60.25	53	4.9	238	44	−89.3	59	46	−90.7	148.0	1.0	328.9	89.0	67	ISC
88/07/12	11.04	−62.96	15	5.1	104	50	−166.2	5	79.4	−40	60.5	19	316.2	35.7	68	CMT
89/01/30	7.80	−72.17	11.2	4.4	46	50	58.2	270	49.4	122.2	157.9	0.3	248.6	66.2	69	Mendoza, 1989
89/04/15	8.50	−60.32	18.5	5.8	194	29	−153	80	77.3	−63.7	149.3	27.6	19.6	50.7	70	CMT
89/04/30	11.10	−68.18	11.1	5.7	167.9	62.7	−177.3	259.2	87.6	−27.3	126.3	18.9	29.5	18.9	71	Malavé, 1992
89/04/30	11.10	−68.18	11.1	5.7	178.1	52.9	−170.6	273.8	82.5	−37.5	139.5	25.2	36.7	25.2	72	Malavé, 1992
89/04/30	11.10	−68.18	11.1	5.7	167.2	67.8	−158.0	265.9	69.7	−23.8	123.8	13.7	29.5	17.3	73	Malavé, 1992
89/05/04	11.14	−68.21	13.6	5.0	137.2	74.2	−168.7	230.3	79.1	−16.1	93.3	11.1	1.1	11.1	74	Malavé, 1992
89/05/04	11.14	−68.21	13.6	5.0	163.5	54.8	−86	336.5	35.4	−95.7	250.6	9.7	89.8	79.7	75	Malavé, 1992
90/C[c]	10.8	−65.50	15	3−5.8	81	70	180	171	90	20	37.8	14	304.2	14	76	Pérez et al., 1997b
90/03/21	10.72	−65.36	32.4	5.2	109	62	−36.3	218	58.5	−146.6	72.1	44	164.2	21	77	Ramos and Mendoza, 1993
91/08/07	9.99	−69.992	18.2	5	45	70	−141.9	300	54.6	−24.8	169.4	9.7	267.8	40.7	78	Valera, 1995
91/08/17	10.003	−70.032	16.2	5.3	310	45	−35.8	67	65.6	−129.1	184.1	12	290.1	52.4	79	Valera, 1995[b]
91/08/17	9.74	−69.83	15	5.5	344	86	0	74	90	−176	200.9	2.8	299.1	2.8	80	CMT
91/08/17	10.54	−62.20	45.2	5.3	124	14	−48.9	262	79.5	−99.3	359.9	33.9	160.6	51.6	81	CMT
91/08/20	10.05	−70.10	1.8	4.5	19	68	174.7	111	85.1	22.1	337.1	19	243	11.8	82	Romero, 1993
91/08/20	10.054	−70.105	1.8	4.5	331	42	−18.5	75	77.7	−130.5	194.7	22	306.5	42.5	83	Valera, 1995[b]
91/08/20	9.988	−70.014	18	4.2	345	40	−10.4	83	83.3	−129.5	203.5	27.4	317.8	38.6	84	Valera, 1995[b]
91/08/21	10.038	−70.032	15.1	4.5	75	75	−126.9	326	39.5	−24	192.1	21.3	306.6	46.8	85	Valera, 1995[b]
91/08/21	10.03	−70.03	15.1	4.5	30	55	−20.3	132	73.5	−143.2	256.4	11.8	356.5	37.4	86	Romero, 1993
91/09/02	10.063	−70.032	7.9	4.7	0	45	12.6	261	81.1	134.3	209.5	37.5	318.6	23	87	Valera, 1995[b]
91/09/14	10.021	−70.041	9.3	4.1	280	65	123.1	43	40.6	40.5	234.7	56.7	346.6	13.8	88	Valera, 1995[b]
91/09/14	10.02	−70.41	41	4.1	37	66	−6.0	130	84.8	−149	259.7	16.8	357.7	24.7	89	Romero, 1993
94/05/31	7.423	−72.001	13.5	6.1	63	75	−128.5	315	40.9	−23.3	181.1	20.6	293.8	45.8	90	Rodríguez, 1995[b]
94/11/09	7.53	−71.73	21.3	5.2	178	42	112.4	329	51.8	71.1	100.7	74.4	72.3	5	91	CMT
95/C[c]	10.2	−67.90	15	3–4.0	0	80	16	267	73.5	169.6	224.3	18.9	132.8	4.5	92	Pérez et al., 1997b[c]
95/12/29	9.99	−70.08	16.2	5.1	47	65	103.7	197	28.3	63.1	342.6	67.1	126.8	18.9	93	Acosta et al., 1996
95/12/29	9.99	−70.08	16.2	5.1	47	65	155.3	148	67.7	27.2	8.2	34.5	277	1.8	94	Audemard et al., 1999
95/12/31	9.86	−69.91	15	5.1	257	74	−176.4	166	86.5	−16	212.6	8.7	120.4	13.8	95	CMT
97/04/15	10.69	−69.63	15	5.2	109	65	163.8	206	75.4	25.9	69.6	28.5	335.8	6.9	96	CMT

(continued on next page)

Table 3 (*continued*)

Date (yy/mm/dd)	Latitude (deg)	Longitude (deg)	Focal depth (km)	Magnitude (mb)	Nodal plane A			Nodal plane B			*T* axis		*P* axis		Fig. 5 label no.	Reference
					AZI	DIP	RAKE	AZI	DIP	RAKE	AZI	DIP	AZI	DIP		
97/07/09	10.545	−63.515	9.41	6.9	270	75	−136.1	166	47.9	−20.4	32.2	16.9	137.5	41.1	97	Audemard et al., 1999
00/10/04	11.016	−62.30	119	6.0	90.0	58	78.5	291	33.8	107.7	328.8	74.2	188.3	12.3	98	Sobiesiak et al., 2002
01/10/31	10.729	−67.016	6.6	3.8	55.0	45	20.8	311	76.6	131.1	261	42.6	9.3	18.8	99	this paper
02/04/01	10.095	−69.07	0.0	3.4	3.0	49	9.1	267	83.1	138.6	216.4	33.3	322	22.3	100	this paper
02/04/12	9.609	−69.996	18.5	4.4	60	70	0.0	330	90	−20	16.8	14	283.2	14	101	this paper
02/04/14	10.158	−67.919	5.5	3.5	262	71	−146.9	160	58.9	−22.4	28.7	7.8	124.5	36.6	102	this paper
02/04/18	12.033	−69.459	30.2	4.2	28	47	0.0	298	90	137	244.2	28.8	351.8	28.8	103	this paper
02/04/18	10.199	−64.91	0.0	4.0	30	40	35.9	271	67.9	124.2	223.4	53.9	336.6	16	104	this paper
02/04/27	10.49	−63.762	2.9	3.7	82	75	−125.4	332	38.1	−24.8	198.2	21.9	314.5	47.7	105	this paper
02/05/27	10.698	−67.995	12	3.5	122	49	−69.3	272	45	−112.2	197.5	2	100.3	74.4	106	this paper
02/05/28	10.638	−66.813	9	3.4	90	40	176.1	183	87.5	50.1	59.4	34.9	304.9	30.7	107	this paper
02/05/28	12.201	−70.065	18.7	4.3	320	74	−49.7	68	42.9	−156.1	21.1	18.9	270.7	45.5	108	this paper
02/06/02	10.383	−67.116	1.4	4.0	72	63	100.9	229	29	69.6	5	70	153.9	17.3	109	this paper
02/06/02	10.358	−67.094	3.9	3.4	206	58	7.5	112	83.6	147.8	64.1	26.9	163.2	17.2	110	this paper
02/06/03	10.402	−67.106	4.7	3.6	38	85	0.0	128	90	−175	262.9	3.5	353.1	3.5	111	this paper
02/06/10	10.189	−67.677	1.2	4.1	260	66	−144.8	154	58.2	−28.6	25.5	4.9	119.7	41.3	112	this paper
02/06/21	9.756	−69.264	4.8	4.0	60	71	159.3	157	70.5	20.2	18.4	27.8	108.6	0.3	113	this paper
02/06/21	9.656	−69.303	0.0	4.1	4	47	64.5	219	48.7	114.8	199.1	71.6	291.7	0.9	114	this paper
02/10/04	10.404	−62.425	8	4.0	195	47	8.8	99	83.6	136.7	47.4	34.1	154.8	23.8	115	this paper
02/10/10	9.899	−69.950	0.3	3.4	52	48	152.8	161	70.1	45.4	25.8	45.5	281.7	13.5	116	this paper
02/10/15	10.531	−63.691	1.6	4.7	190	48	8.9	94	83.4	137.7	42.9	33.7	149.4	23.1	117	this paper
02/11/28	10.878	−62.233	60.7	4.0	308	22	0.0	218	90	−68	287.5	41	148.5	41	118	this paper
02/12/04	10.814	−62.573	77.5	4.2	86	42	−82.5	256	48.4	−96.7	305.7	3.2	113.5	84.1	119	this paper
03/01/07	9.83	−69.987	0.2	4.0	313	45	0.0	223	90	135	168.3	30	277.7	30	120	this paper
03/01/15	8.876	−70.223	12.6	4.2	260	50	128.4	29	53.1	53.5	237.1	61.5	143.9	1.7	121	this paper
03/02/11	10.213	−67.204	00	3.1	73	84	118.3	174	28.8	12.5	10.7	43.9	139.4	33.1	122	this paper
03/02/18	8.975	−70.609	0.1	3.7	44	67	180	134	90	23	1.4	16	266.6	16	123	this paper
03/04/01	9.838	−70.819	0.1	3.2	39	67	131.3	153	46.2	32.8	355.5	50	100.5	12.3	124	this paper
03/04/01C	9.817	−70.804			34	63	131.7	151	48.3	37.4	354.3	52.3	95.6	8.6	125	this paper

ISC=International Seismological Center; CMT=Centroid Moment Tensor.

[a] Reassessed by G. Romero.

[b] Modified by Audemard et al. (1999b).

[c] 88/09/12C, Composite Focal Mechanism.

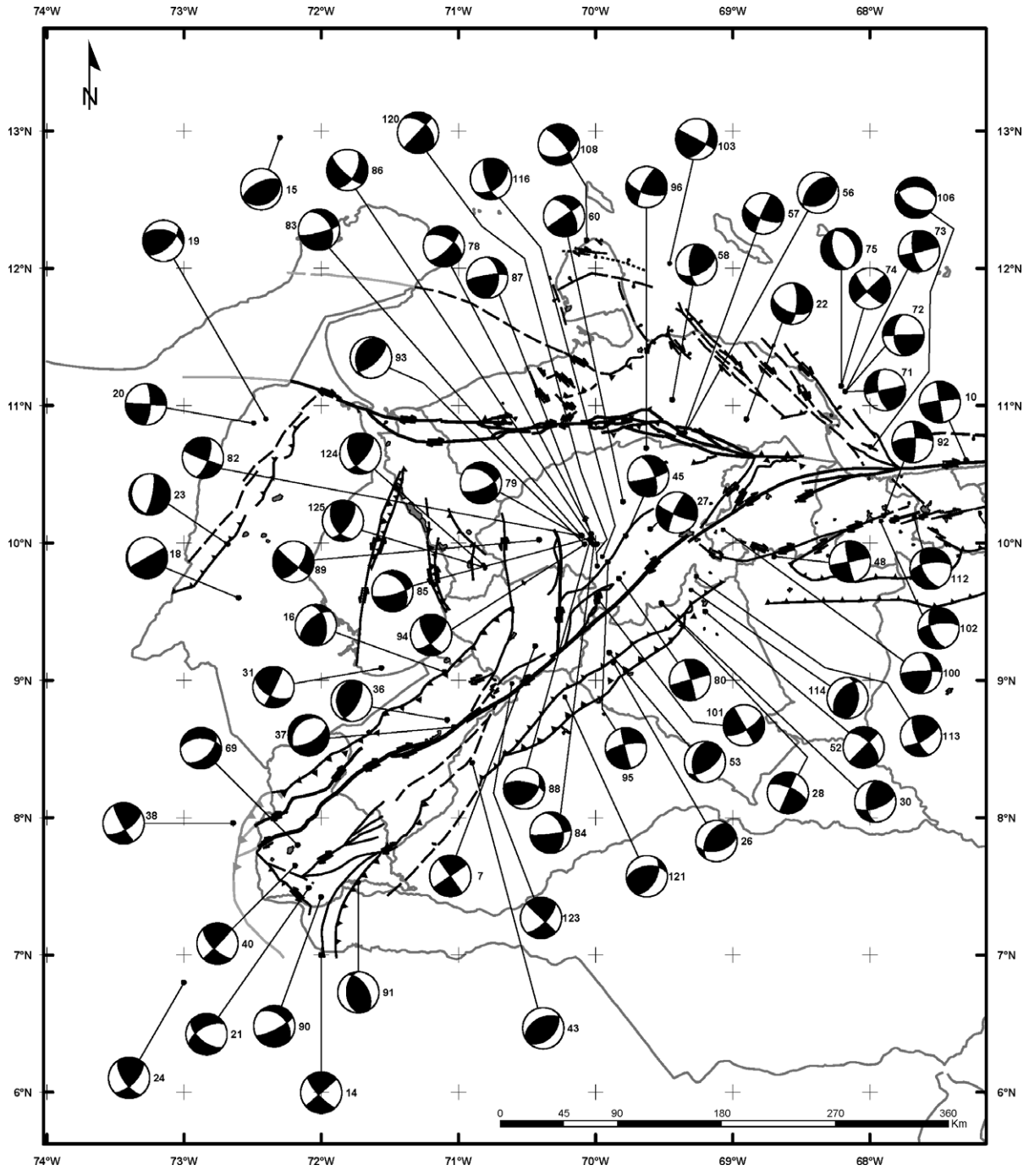

Fig. 6. Compilation map of focal mechanism solutions for Venezuela. Except for the southern end of the Lesser Antilles subduction and few scattered Netherlands Antilles slab-related earthquakes in northwestern Venezuela, all solutions correspond to crustal earthquakes (updated and modified from Audemard et al., 1999). Tensor labelling corresponds to the numbers in Table 3. This map is fractioned regionally in three (a through c): western, central and eastern Venezuela. The tectonic base map corresponds to the one displayed in Figs. 2 and 3 (for toponyms, refer to those figures).

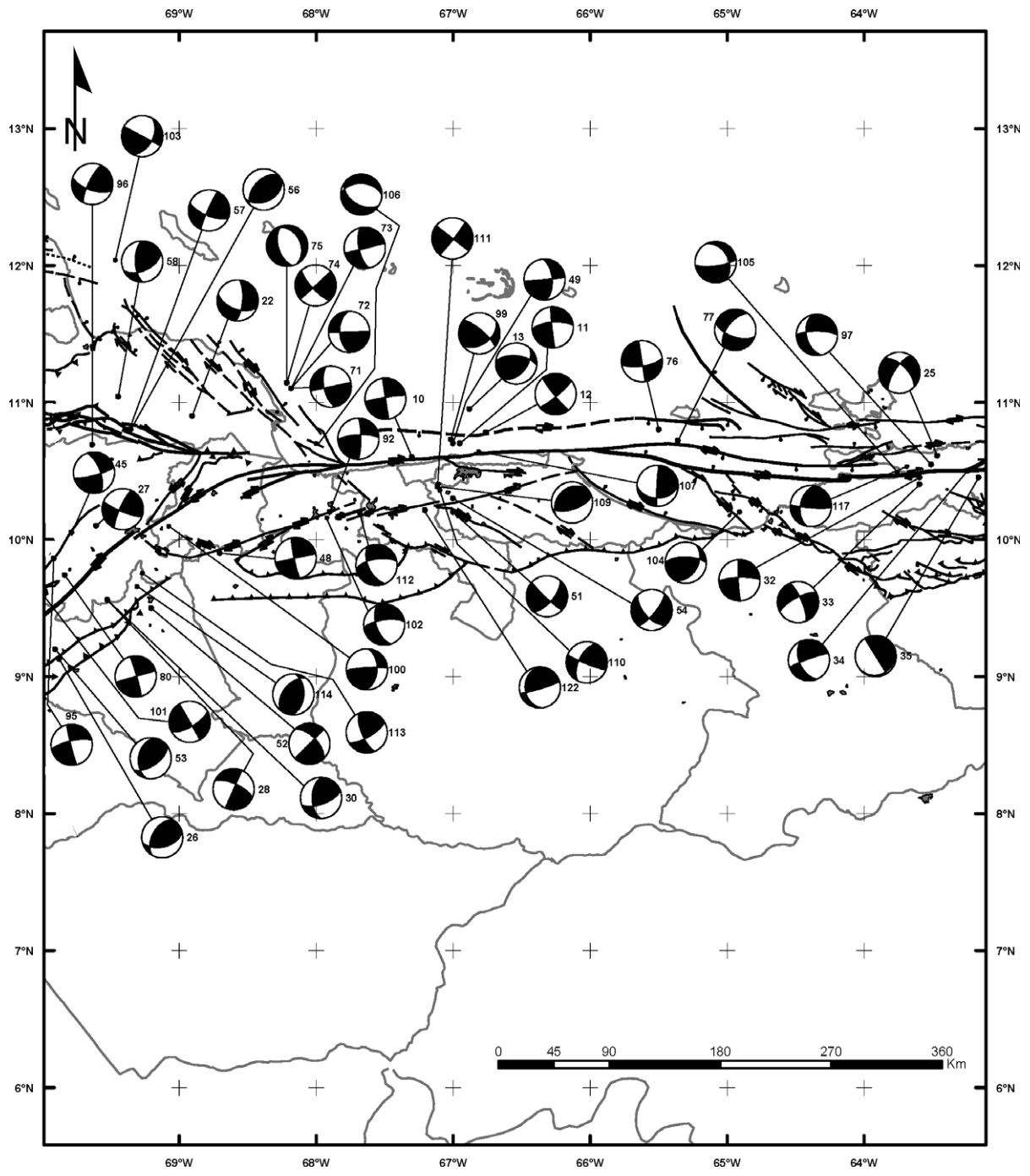

Fig. 6 (*continued*).

consistency and persistency in *P* and *T* axis orientations throughout northern Venezuela (Fig. 6). The *P* and *T* axes respectively trend NW–SE to NNW–SSE (N145° to 170°) and NE–SW to ENE–WSW. No focal mechanism inversion has been performed for this paper, by applying a method such as the Angelier and

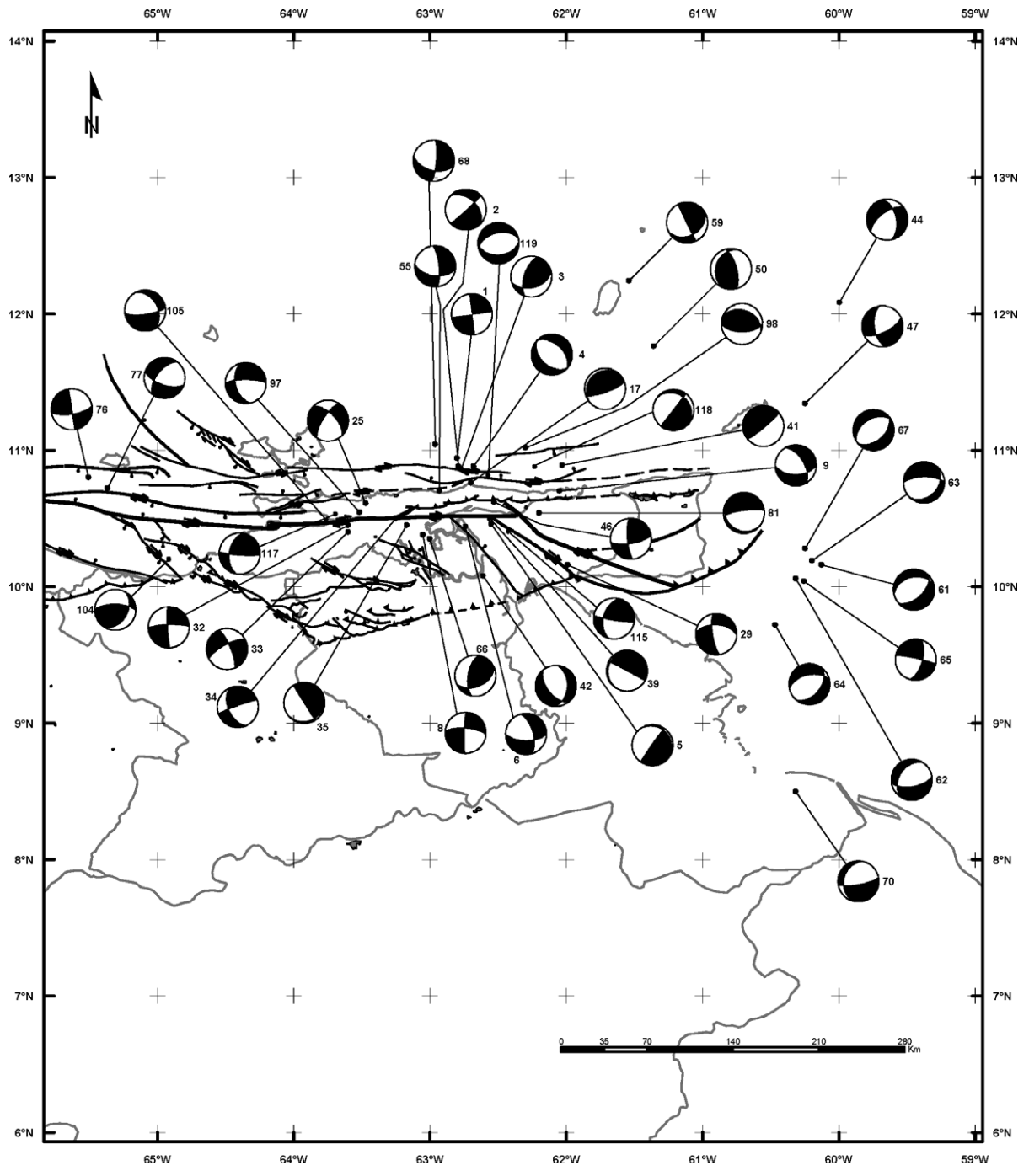

Fig. 6 (*continued*).

Mechler's (1977) dihedral method. We plan this as future work, which would allow a direct comparison between the two sets of tensors. Nonetheless, the two sets of independent data, the geologically derived stress tensors and the *P* and *T* axes from fault-plane solutions, seem to reflect the same fault kinematics

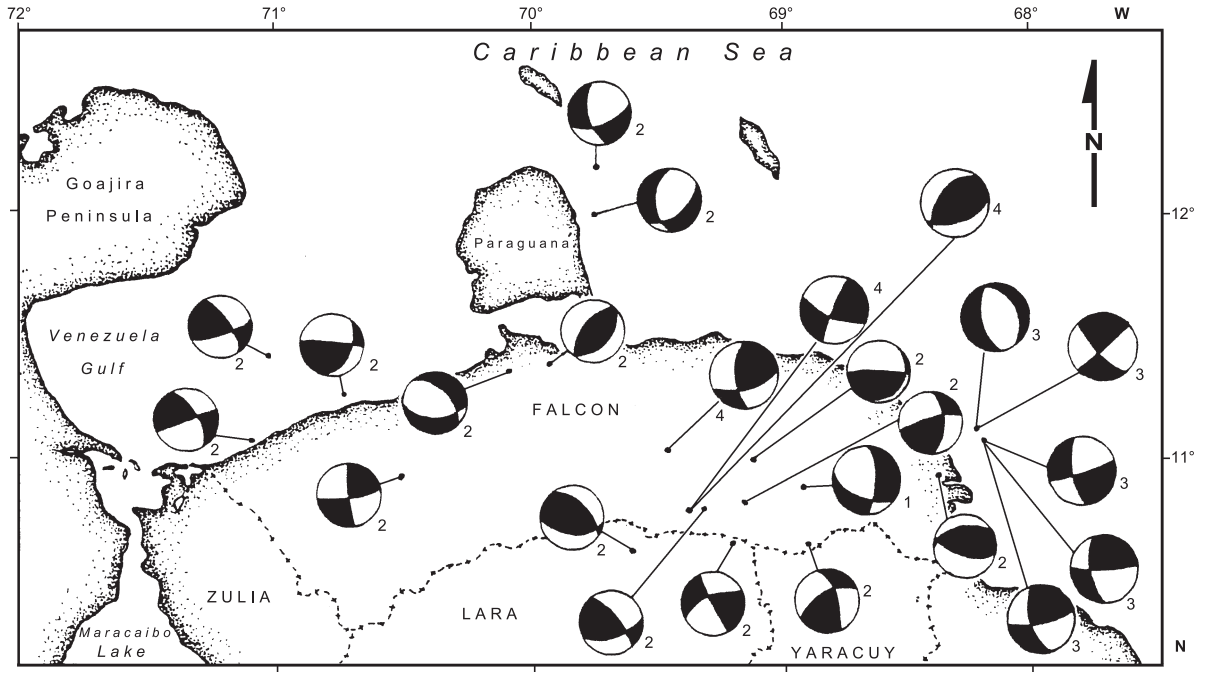

Fig. 7. Focal mechanism solutions for the Falcón region (modified from Audemard et al., 1999). Solutions labelled: (1) is from Dewey (1972) (modified by Audemard and Romero, 1993); (2) were obtained from a microseismicity survey made in 1990 in an Intevep-CEE project (modified from Bach, 1991); (3) are from Malavé (1992); and (4) are from Audemard and Romero (1993).

along this complex plate boundary zone. The focal mechanism *P* and *T* axes match well with the axis orientations of the geologically derived (from both microtectonic and borehole data) stress tensors throughout the region (compare Figs. 5 and 6). Additionally, this comparison is also valid for the Mérida Andes chain at very shallow crustal levels (<40 km deep): the *P* axis trends east–west when nearing the Boconó fault, similar to the maximum horizontal stress derived from microtectonic data (compare Figs. 5a and 6a). Consequently, the focal mechanism solutions give additional supporting evidence to the present activity and kinematics of the seven fault families present along northern Venezuela described in Section 2, as well as to those active faults characterized in the Mérida Andes.

Beyond the crustal deformation described previously by means of their causative stress tensors or their kinematics derived from the rupture nucleation, few intermediate earthquakes, up to 200 km deep, have been detected under lake Maracaibo basin in northwestern Venezuela (Fig. 4B). They have been attributed, using focal solutions (e.g., Dewey, 1972; Kellogg and Bonini, 1982; Malavé and Súarez, 1995; Pérez et al., 1997a) and seismic tomography (Van der Hilst, 1990), either to the SSE-directed oceanic slab of the Leeward Antilles subduction (LAS in Fig. 1) or to its western extension. This prolongation bends around northwestern South America until it strikes north–south and gently dips east under Colombia. Since our prime aim in this paper is to determine the present-day tectonic regime at crustal level, only three focal mechanism solutions related to the LAS are included in this compilation (focal solutions labelled 15, 18 and 23 in Table 3 and Fig. 6a). The solution labelled 15 (at 58 km deep) images the compressive regime at the coupled zone between both plates, whereas the two other solutions depict the moment-bending normal faulting occurring at around 150 km in depth.

When addressing present southern Caribbean seismotectonics, it is impossible to skip the intermediate-depth seismicity under Trinidad, the Paria peninsula and the gulf of Paria. Both shallow and intermediate depth earthquake focal mechanisms in the latter region are herein presented to define where the main wrenching within the plate boundary zone should be

(Los Bajos–El Soldado normal–dextral fault system), splitting apart crustal earthquakes on the southwest (Fig. 4A) from the slab-related earthquakes of the southern tip of the type-B Lesser Antilles subduction (Fig. 4B). This boundary is more precisely revealed by comparing the seismicity distribution in eastern Venezuela and Trinidad, shown in Fig. 4A and B.

In the same way that Malavé and Súarez (1995) have proposed the occurrence of slab pull effect based on the intermediate-depth earthquakes under the Perijá range (in western Venezuela) and northern Colombia, Choy et al. (1998) has imaged it at the southern tip of the Lesser Antilles subduction, under the volcanic arc (similar to mechanisms 41 and 81 of Fig. 6c and Table 3). Moreover, in the same region but at shallower depth (between 30 and 70 km deep), a set of focal mechanisms (44, 47, 61 through 64 of Fig. 6c and Table 3, among others; also in Fig. 3 of Choy et al., 1998) attest to moment bending normal faulting of the outer upper edge of the subducting slab at such depth.

At more local scale, some tectonic processes or stress perturbations can also be derived from the evaluation of certain focal solutions, in the same way that the evaluation of the microtectonically derived stress tensors can (as discussed in Section 4):

(a) Laffaille (1981) generates two closely located but very different focal mechanisms: one for each of the valleys of the Mucujún and Chama rivers, respectively (locations given by focal solutions 36 and 37 in Fig. 6a). The first of the two (solution 36) corresponds to north–south reverse faulting paralleling the Mucujún valley, whereas the second to NE–SW-trending normal faulting paralleling the Chama valley and the Boconó fault. The first tensor fits the regional stress field (east–west trending ς_H), whereas the second images local transtension, as should be expected along this portion of the Boconó fault, where the fault steps across the Las González pull apart-basin ("B" in Fig. 2).

(b) When evaluating the Churuguara 1986 seismic swarm, Audemard and Romero (1993) determined the occurrence of dextral reverse slip on a secondary fault to the Oca–Ancón during an aftershock (focal mechanism 58 in Fig. 6a) after dextral slip on the Oca–Ancón fault system during a larger event (mechanism 57 in Fig. 6a).

(c) The low frequency of moderate-to-large earthquakes in Venezuela, and the consequent little generation of focal mechanisms solutions before the very recent seismological network modernization, has been partly overcome by making composite focal mechanism solutions from earthquake sets tightly gathered in space and time. They have mostly confirmed the fault kinematics established via geologic criteria (Laffaille, 1981; Pérez and Aggarwal, 1981; Ramos and Mendoza, 1991; Audemard and Romero, 1993; Pérez et al., 1997a,b; Jaimes et al., 1998).

(d) Ramos and Mendoza (1993) proposed a focal solution for the march 21, 1990 earthquake, located south of the Tortuga island. This solution images (solution 77 in Fig. 6b and Table 3) east–west-trending normal faulting, which supports the kinematics of the San Sebastián/El Pilar fault relay where the Cariaco trough pull-apart basin is forming. Then, the northern border normal fault of the basin slipped.

6. Discussion

Active fault kinematics derived from focal mechanisms solutions of crustal (<30 km deep) earthquakes along the plate boundary zone, in northern and western Venezuela, is in good agreement with geologic fault-plane kinematic-indicators. This fact could also be inferred by simply comparing *P* and *T* axis orientations from focal solutions with the principal horizontal stress orientations derived from geologic (microtectonic and borehole) data. Although this comparison should be avoided because both dataset are not equivalent, this implies that *P* axis orientations from focal mechanism solutions coincide pretty well with the maximum horizontal stress trajectories derived from microtectonically derived stress tensors (compare Figs. 5 and 6). This affirmation will only be firmly confirmed after focal mechanism inversions are made. However, the common intersection resulting from mentally adding the *P* area(s) of closely gathered focal mechanism solutions, as well as the *T* area(s), which defines respectively the most likely common maximum and minimum horizontal stress orientations of those solutions, foresees that matching between stress tensors derived from both datasets should be very close.

Throughout northern Venezuela, the comparison of both datasets (kinematics from focal mechanism solutions and stress tensors from microtectonic data) allows to gather active faults in seven main fault

trends: (a) east–west right-lateral faults; (b) NW–SE right-lateral faults, synthetic to the east–west faults; (c) NNW–SSE normal faults; (d) NW–SE to NNW–SSE normal–dextral to dextral–normal faults; (e) North–South to NNE–SSW left-lateral faults, antithetic to the east–west faults, with the rare exception of the ENE–WSW-trending Punta Charagato and Laguna Grande faults; (f) ENE–WSW to east–west right-lateral faults—P shears; and (g) ENE–WSW reverse faults, parallel to folding axis. In the Mérida Andes of western Venezuela, our conclusion is that active partitioning is taking place: NE–SW trending dextral wrenching along the Boconó and minor parallel faults simultaneous with normal-to-chain shortening (vertical growth through folding and thrusting). The new focal mechanism solutions presented herein bring additional supporting evidence to the ongoing partitioning hypothesis originally proposed from geologic data (Audemard and Audemard, 2002). These focal solutions show mainly pure strike or reverse slip in this region (Fig. 6a). A recent compilation of focal solutions for the northern Mérida Andes made by Palme et al. (2001) also reached the same conclusion. Though the number of focal mechanism solutions for the entire Mérida Andes is not large (Fig. 6a), it distinctly shows that wrenching essentially occurs along the chain axis, whereas three mechanisms (solutions 26, 30 and 53 in Fig. 6a and Table 3) on the eastern side of the Andes (among them: the Guanare 1975 and the Ospino 1977 earthquakes) show dominant reverse slip.

From the geologic data inversion, northern Venezuela is undergoing a compressive-transcurrent (transpressional s.l.) regime characterized by maximum and/or minimum horizontal stresses trending NNW–SSE to NW–SE and ENE–WSW to NE–SW, respectively. This is further supported by slip vectors in eastern Venezuela derived by Pérez et al. (2001). Furthermore, the magnitude and orientation of those vectors, besides confirming the active transpression, are in pretty good agreement with the slip rates of the major active faults in that region proposed from geologic criteria (compare with slip rates in Audemard et al., 2000). As well as in central Venezuela, wrenching is the dominant process in eastern Venezuela, with a slip rate concentrated on the El Pilar fault in the order of 8–10 mm/year, but other minor faults with various orientations, including subparallel faults and even slightly oblique thrust faults to the main dextral system, slip an order of magnitude less faster (<1–2 mm/year). Slip of such a magnitude cannot be yet resolved by GPS data, because the fault slip rates is within the average GPS velocity errors (ρ1–2 mm/year) indicated for the South American sites by Weber et al. (2001a). Longer GPS records, over one to two decades long, are in need to be able of determining accurately so slow slip rates.

The Mérida Andes is also subject to a similar stress tensor of the compressive-transcurrent type but σ_H is rotated to an east–west orientation. Meanwhile, σ_H shows an intermediate orientation between the Andes and northern Venezuela regions. This suggests that the stress field turns counter-clockwise, as originally proposed by Giraldo and Beltrán (1988; Fig. 8). The bending of the trajectories proposed herein is however more pronounced than those of Giraldo and Beltrán (1988) when crossing the Mérida Andes axis. This has also been determined by Palme et al. (2001) for the northern Mérida Andes, between the Valera and Boconó faults. As well, the maximum horizontal stress trajectories in this paper along northern Venezuela trend almost normal to the east–west-trending wrenching system, supporting ongoing transpression. Although wrenching in the Andes is also the prevailing active deformational mechanism, shortening across the chain seems much more important here than along northern Venezuela. This argument is supported, besides the present relief of the chain reaching almost 5000 m in elevation, by the geologically derived slip rates of both foothills thrust fault systems, which slip at about 0.5 mm/year.

7. Conclusions

An integrated compilation of microtectonic (fault-plane kinematic indicators) analyses, borehole data and focal mechanism solutions, complemented by regional neotectonic assessments, show that strain along northern and western Venezuela at present is being partitioned along the entire active plate boundary zone. On one hand, deformation along the southern Caribbean coast results from a compressive strike-slip (transpressional s.l.) regime characterized by a NNW–

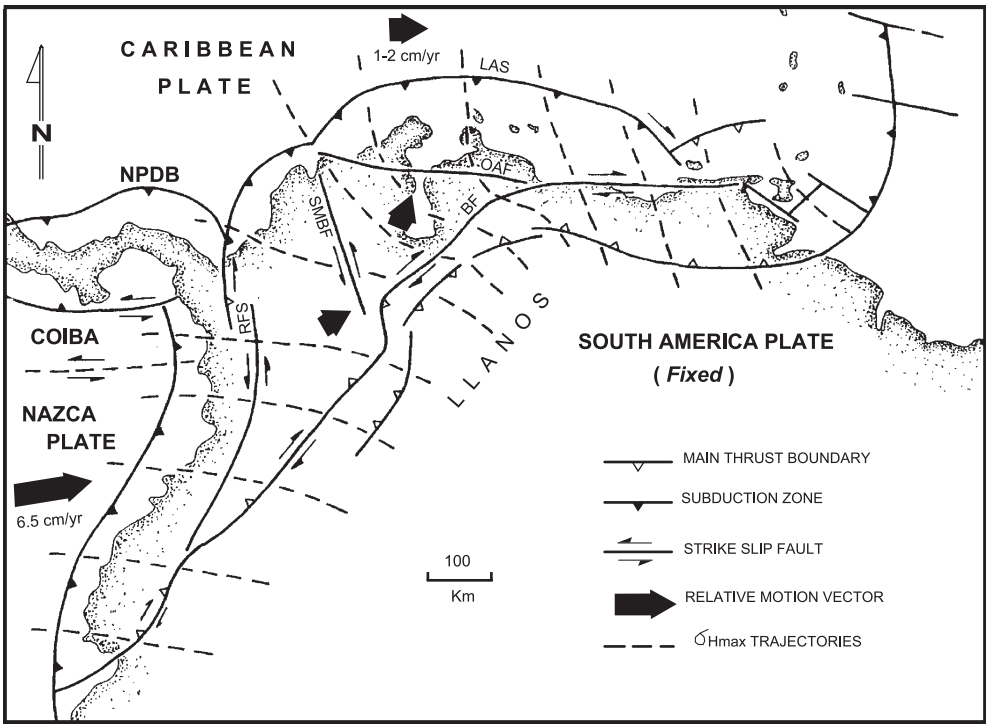

Fig. 8. Maximum horizontal stress trajectories for northern South America, based on neotectonic data, fault-plane kinematic indicators and focal mechanism solutions. Legend: BF: Boconó fault, LAS: Leeward Antilles subduction, OAF: Oca–Ancón fault, RFS: Romeral fault system, SMBF: Santa Marta–Bucaramanga fault (modified from Audemard and Audemard, 2002).

SSE maximum horizontal stress (ς_H=ς_1) and/or an ENE–WSW minimum (ς_h=ς_3 or ς_2) horizontal stress, which is responsible for present activity and kinematics of seven sets of structural—both brittle and ductile—features: east–west right-lateral faults (Oca–Ancón, San Sebastián, El Pilar, Northern Coast), NW–SE right-lateral faults—synthetic Riedel shears (Urumaco, Río Seco, La Soledad, Costa Oriental de Falcón, Río Guarico, Tácata, Aragüita, Píritu, Urica, San Francisco, Los Bajos–El Soldado), ENE–WSW to east–west dextral faults—P shears (La Victoria fault), NNW–SSE normal faults (Costa Occidental de Paraguaná, Los Médanos, Río San Juan Graben, Bohordal), almost north–south left-lateral faults—antithetic Riedel shears (Carrizal, Quebrada Chacaito), ENE–WSW reverse faults—sub-parallel to fold axes and mostly in the subsurface (Matapalo, Taima-Taima, Cantagallo, Tala, Interior range frontal thrusts, Tunapuy) and associated ENE–WSW-trending folding (well-developed in the Falcón basin—northwestern Venezuela—and the Interior range in the east). The main exceptions to this general configuration are found in eastern Venezuela: the Punta Charagato and Laguna Grande faults, at Punta Charagato (northern Cubagua island) and Araya Peninsula, respectively, that display left-lateral slip along the ENE–WSW direction. In most of northern Venezuela, brittle deformation obeys the simple shear model.

On the other hand, the stress field on the Maracaibo block and south of the Oca–Ancón fault progressively turns counter-clockwise to become more east–west oriented, allowing left- and right-lateral slip along the north–south-striking (e.g., Valera and Burbusay) and NE–SW-striking (e.g., Boconó, Caparo, Queniquéa, San Simón) faults, respectively. This regional stress field in western Venezuela results from the superposition of the two major neighbouring interplate maximum horizontal stresses (ς_H): east–west trending stress across the Nazca–South America type-B suduction along the pacific coast of Colombia and NNW–SSE oriented one across the Caribbean southern boundary. Therefore, the Maracaibo block is

simultaneously being shortened on the NW–SE direction (expressed by the vertical growth of the Santa Marta block and Perijá and Mérida ranges) and extruded roughly towards NNE.

The stress tensors derived from geologic (microtectonic and borehole) data compiled herein, as well as the *P* and *T* axis orientations from focal mechanism solutions, seem in good agreement with recent slip vectors derived from several GPS studies performed both in western and eastern Venezuela, essentially during the 1990s. Wrenching is the dominant geodynamic process, but it is always accompanied by compression of variable magnitude along strike of the major strike-slip fault system comprising the Boconó, San Sebastián and El Pilar faults. Only locally, transtension becomes significantly important, such as in the Cariaco trough and gulf of Paria in association with the El Pilar fault. Furthermore, the GPS slip vectors do not only support the hypothesis of ongoing transpression along most of this complex plate boundary zone, but also tend to confirm most of the active fault slip rates derived from geologic and neotectonic studies carried out in Venezuela for almost 25 years by Funvisis staff.

Acknowledgements

Comments from John Weber (Grand Valley State University, Allendale, USA) to an earlier version of this manuscript improved this contribution, for which we are very thankful. Our thanks also go to the Managing Editor, Dr. Giuliano F. Panza, for providing helpful recommendations. This publication results from a project financed by PDVSA-CVP, under the leadership of Jairo Lugo. We much appreciate the continuous funding from Funvisis to this fundamental research line of the Earth Sciences Department that allowed most of the dataset collection and generation. Our appreciation also goes to Raymi Castilla (formerly at Funvisis, Caracas, Venezuela) and Guillaume Backe (graduate student at Université de Pau et des Pays de l'Adour, Pau, France) who helped to depurate some typing errors in the focal mechanism dataset. Marina Peña is thanked for her drawings. This paper is a contribution to FONACIT projects G-2002000478 and PI-2003000090, as well as to IGCP-433.

References

Acosta, L., 1995. Estudio geológico en la quebrada de Tacagua. Parte alta. Distrito Federal. Undergraduate thesis, Universidad Central de Venezuela, 213 pp + appendices.

Acosta, L., 1997. Estudio de la traza activa de la falla de Tacagua–El Avila para fines de microzonificación del corredor estratégico Caracas–Litoral Norte–central de Venezuela. Proceedings VIII Congreso Geológico Venezolano, Porlamar, vol. 1, pp. 21–27.

Acosta, L., Arzola, A., Hernández, A., Grimán, C., 1996. El sismo de Los Arangues del 29 de Diciembre de 1995. Unpublished FUNVISIS' report, 54 pp.

Aggarwal, Y., 1983. Neotectonics of the Southern Caribbean: recent data, new ideas. Acta Científica Venezolana 34 (1), 17. (abstract).

Angelier, J., 1994. Fault slip analysis and paleostress reconstruction. In: Hancock, P. (Ed.), Continental Deformation. Pergamon, Oxford, pp. 53–100.

Angelier, J., Mechler, P., 1977. Sur une méthode graphique de recherche des contraintes principales également utilisable en tectonique et séismologie: la méthode des diedres droits. Bulletin de la Société Géologique de France 19 (6), 1301–1318.

Audemard, F.A., 1984. Evaluación geológica de la Cuenca del Tuy para fines de investigaciones neotectónicas. Undergraduate thesis, Universidad Central de Venezuela. 226 pp + appendices. 2 Vol.

Audemard, F.A., 1985. Neotectónica de la Cuenca del Tuy. Proceedings VI Congreso Geológico Venezolano, Caracas, vol. 4, pp. 2339–2377.

Audemard, F.E., 1991a. Tectonics of Western Venezuela. PhD thesis. Rice University, 245 pp + appendices.

Audemard, F.A., 1991b. Proyecto suministro Falcón–Zulia (SUFAZ): Actividad cuaternaria y caracterización sismogénica de las fallas de Lagarto y Rio Seco. Afinamiento de las características sismogénicas del sistema de fallas de Oca–Ancón y de Urumaco. Unpublished Funvisis' report for Maraven; 91 pp + appendices.

Audemard, F.A., 1993. Néotectonique, Sismotectonique et Aléa Sismique du Nord-ouest du Vénézuéla (Système de failles d'Oca–Ancón). PhD thesis, Université Montpellier II, France, 369 pp + appendix.

Audemard, F.A., 1996. Paleoseismicity studies on the Oca–Ancon fault system, northwestern Venezuela. Tectonophysics 259, 67–80.

Audemard, F.A., 1997a. Holocene and Historical Earthquakes on the Boconó Fault System, Southern Venezuelan Andes: trench confirmation. Journal of Geodynamics 24 (1–4), 155–167.

Audemard, F.A., 1997b. Tectónica activa de la región septentrional de la cuenca invertida de Falcón, Venezuela occidental. Proceedings VIII Congreso Geológico Venezolano, Porlamar, vol. 1, pp. 93–100.

Audemard, F.A., 1998. Evolution Géodynamique de la Façade Nord Sud-américaine: Nouveaux apports de l'Histoire Géologique du Bassin de Falcón, Vénézuéla. Proceedings XIV Caribbean Geological Conference, Trinidad, 1995, vol. 2, pp. 327–340.

Audemard, F.A., 1999a. El sismo de Cariaco del 09 de julio de 1997, edo. Sucre, Venezuela: nucleación y progresión de la

ruptura a partir de observaciones geológicas. Proceeedings VI Congreso Venezolano de Sismología e Ingeniería Sísmica, Mérida, in CD-Rom.

Audemard, F.A., 1999b. Morpho-structural expression of active thrust fault systems in the humid tropical foothills of Colombia and Venezuela. Zeitschrift für Geomorphologie 118, 1–18.

Audemard, F.A., 1999c. Nueva percepción de la sismicidad histórica del segmento en tierra de la falla de El Pilar, Venezuela nororiental, a partir de primeros resultados paleosísmicos. Proceedings VI Congreso Venezolano de Sismología e Ingeniería Sísmica, Mérida, in CD-Rom.

Audemard, F.A., 2000a. Neotectónica de la Cuenca del Tuy: Observaciones complementarias. Memorias de las Jornadas Científicas 55 Aniversario Escuela de Geología, Minas y Geofísica, 1938–1993, Caracas, Boletín GEOS 32 (Diciembre 1997), 39–42.

Audemard, F.A., 2000b. Major Active Faults of Venezuela. Proceedings 31st International Geological Congress, Rio de Janeiro, Brasil, 4pp. (extended abstract; in CD-Rom).

Audemard, F.A., 2001. Quaternary tectonics and present stress tensor of the inverted northern Falcón Basin, Northwestern Venezuela. Journal of Structural Geology 23, 431–453.

Audemard, F.A., 2002. Ruptura de los grandes sismos históricos venezolanos de los siglos XIX y XX revelados por la sismicidad instrumental contemporánea. Proceedings XI Congreso Venezolano de Geofísica, 8 pp. (CD-Rom format).

Audemard, F.A., Arzola, A., 1995. Evaluación de la actividad tectónica de las fallas de sitio para el proyecto Terminal de Almacenamiento y Embarque de Crudo por Jose—TAECJ, Fase II (Jose, Edo. Anzoátegui). Unpublished Funvisis' report for CORPOVEN, 32 pp + appendices.

Audemard, F.E., Audemard, F.A., 2002. Structure of the Mérida Andes, Venezuela: relations with the South America–Caribbean geodynamic interaction. Tectonophysics 345, 299–327.

Audemard, F.E., De Mena, J., 1985. Falcón oriental, nueva interpretación estructural. Proceedings VI Congreso Geológico Venezolano, pp. 2317–2329.

Audemard, F.A., Romero, G., 1993. The Churuguara area—Seismic evidence of contemporary activity of the Oca–Ancón system. Proceedings, Caribbean Conference on Natural Hazards: Volcanoes, Earthquakes, Windstorms, Floods. St. Augustine, pp. 21–32.

Audemard, F.A., Singer, A., 1996. Active fault recognition in northwestern Venezuela and its seismogenic characterization: neotectonic and paleoseismic approach. Geofísica Internacional 35, 245–255.

Audemard, F.A., Singer, A., 1997. La Ingeniería de Fallas Activas en Venezuela: historia y estado del arte. Seminario Internacional de Ingeniería Sísmica: Aniversario del Terremoto de Caracas de 1967. Universidad Católica Andrés Bello, Caracas, pp. 11–27.

Audemard, F.A., De Santis, F., Lugo, M., Singer, A., Costa, C., 1988. Sismotectónica y Sismicidad Histórica, In Singer, A. (coord.): Estudio de Amenaza Sísmica para las Urbanizaciones La Punta y Mata Redonda, al Sur de Maracay. Unpublished Funvisis' report for MINDUR. 2 Vol.

Audemard, F.A., Singer, A., Beltrán, C., Rodríguez, J.A., Lugo, M., Chacín, C., Adrianza, A., Mendoza, J., Ramos, C., 1992. Actividad tectónica cuaternaria y características sismogénicas de los sistemas de falla de Oca–Ancón (tramo oriental), de la Península de Paraguaná y región de Coro y de la costa nororiental de Falcón. Unpublished Funvisis' report for INTEVEP, Los Teques, 2 Vol., 245 pp.

Audemard, F.A., Beltrán, C., Singer, A., 1993. Evaluación Neotectónica Preliminar de la Galería Superior del Estribo Caracas del Viaducto N° 1 de la Autopista Caracas-La Guaira. Unpublished Funvisis' report for RDS y WS Asesoramientos Técnicos, 19 pp + 3 appendices.

Audemard, F.A., De Santis, F., Singer, A., Ramos, C., 1995. El Sistema de Fallas de La Victoria, Venezuela Norcentral: Trazas Activas, Complejidades Estructurales, Cinemática y Sismicidad Asociada. Proceedings IX Congreso Latinoamericano de Geología, Diskette.

Audemard, F.A., Romero, G., Rendón, H., 1999. Sismicidad, Neotectónica y Campo de Esfuerzos del Norte de Venezuela. Unpublished Funvisis' report for PDVSA-CVP, 221 pp.

Audemard, F.A., Machette, M., Cox, J., Dart, R., Haller, K., 2000. Map and Database of Quaternary Faults and Folds in Venezuela and its Offshore Regions. USGS Open-File report 00-0018 (accessible from USGS webpage; open file reports ofr-00-0018).

Audemard, F.A., Castilla, R. and Malavé, G. 2003. Eventuales deformaciones permanentes de origen cosísmico en un área costera ubicada al SW de Güiria, estado Sucre: evaluación preliminar. VII Congreso Venezolano de Sismología e Ingeniería Sísmica (CD-Rom format).

Bach, B., 1991. Interpretation und Analyse tektonischer Prozesse anhand mikroseismicher Messungen im Estado Falcon, nordvenezuela. Master thesis, Universitat Hamburg, 95 pp.

Bach, B., Muñoz, M., Franke, M., Villaseñor, A., Gajardo, E., 1992. Estudios de microsismicidad en el norte de Venezuela: 2. zona noroccidental. Proceedings VI Congreso Venezolano de Geofísica, Sociedad Venezolana de Ingenieros Geofísicos, pp. 522–528.

Badell, C., 1981. El terremoto de San Pablo del 05 de Abril de 1975. Proceedings III Congreso Venezolano de Sismología e Ingeniería Sísmica, Caracas, pp. 257–273.

Beck, C., 1979. New data about recent tectonics in the central part of the Caribbean chain: the Santa Lucía–Ocumare del Tuy graben, Miranda State, Venezuela. Proceedings IV Latin American Geological, pp. 59–68.

Beck, C., 1986. Géologie de la Chaîne Caraïbe au méridien de Caracas (Venezuela). Pubication-Societé Géologique du Nord 14, 462 pp.

Bell, J., 1972. Geotectonic evolution of the southern Caribbean area. Memoir-Geological Society of America 132, 369–386.

Beltrán, C. (comp.), 1993. Mapa Neotectónico de Venezuela. Escala 1: 2,000,000. Funvisis.

Beltrán, C., 1994. Trazas activas y síntesis neotectónica de Venezuela a escala 1:2.000.000. Proceedings VII Congreso Venezolano de Geofísica, Caracas. 541–547.

Beltrán, C., 1998. Preliminary observations on Quaternary reverse faulting along the southern foothills of the Northern Range of Trinidad. Proceedings XIV Caribbean Geological Conference, Trinidad, 1995, vol. 1, pp. 233–239.

Beltrán, C., Giraldo, C., 1989. Aspectos neotectónicos de la región nororiental de Venezuela. Proceedings VII Congreso Geológico Venezolano, Barquisimeto, vol. 3, pp. 1000–1021.

Blanco, B., Giraldo, C., 1992. Síntesis tectono-estratigráfica de la cuenca Tuy-Cariaco y plataforma externa. Proceedings VI Congreso Venezolano de Geofísica, Caracas, vol. 1, pp. 47–54.

Blin, B., 1989. Le front de la Chaine Caraïbe Vénézuélienne entre la Serrania de Portuguesa et la region de Tiznados (surface et subsurface): Apport des données paléomagnétiques. Interprétation géodynamique. PhD thesis, Université de Bretagne Occidentale, Brest, France, 389 pp+ appendices.

Boinet, T., 1985. La Frontière Méridionale de la Plaque Caraïbe aux confins Colombo–Venezueliens (Norte de Santander, Colombie): Données Géologiques. PhD thesis, Université Paris VI., 204 pp + appendices.

Bott, M., 1959. The mechanics of oblique slip faulting. Geology Magnetics 96, 109–117.

Carey, E., 1976. Analyse numérique d'un modèle mécanique élémentaire appliqué à l'etude d'une population de failles. Calcul d'un tenseur moyen des contraintes à partir de stries de glissement. PhD Thesis, Université Paris Sud, 138 pp.

CEE-INTEVEP, 1993. Seismotectonic of northern Venezuela (The contact between the Caribbean and South American Plates). Final report, 48 pp + appendices.

Choy, J., 1998. Profundidad y mecanismo focal del terremoto de El Tocuyo, 1950. Revista de Geofísica (Venezolana) 39 (1–2), 203–217.

Choy, J., Morandi, M.T., Palme De Osechas, C., 1998. Determinación de patrones de esfuerzos tectónicos para el Oriente de Venezuela-Sureste del Caribe a partir de mecanismos focales. Proceedings IX Congreso Venezolano de Geofísica, Caracas, CD-Rom; paper no. 17.

Cisternas, A., Gaulon, A., 1984. Síntesis Sismotectónica del nordeste de Venezuela. Revista de Geofísica 40, 3–10.

Cluff, L., Hansen, W., 1969. Seismicity and Seismic-Geology of northwestern Venezuela. Unpublished Woodward-Clyde's report for Shell. 2 volumes.

Colletta, B., Roure, F., De Toni, B., Loureiro, D., Passalacqua, H., Gou, Y., 1996. Tectonic inheritance and structural styles in the Merida Andes (western Venezuela). III International Symposium on Andean Geodynamics (3 ISAG), Saint-Malo, Frrance, pp. 323–326.

Colletta, B., Roure, F., De Toni, B., Loureiro, D., Passalacqua, H., Gou, Y., 1997. Tectonic inheritance, crustal architecture, and contrasting structural styles in the Venezuelan Andes. Tectonics 16 (5), 777–794.

De Toni, B., Kellogg, J., 1993. Seismic evidence for blind thrusting of the northwestern flank of the Venezuelan Andes. Tectonics 12 (6), 1393–1409.

Dewey, J., 1972. Seismicity and tectonics of western Venezuela. Bulletin of the Seismological Society of America 62 (6), 1711–1751.

Espínola, E., Ollarves, R., 2002. Estudio tectono-estratigráfico del borde septentrional de la cuenca de Barlovento, estado Miranda. Implicaciones neotectónicas. Unpublished undergraduate thesis, Universidad Central de Venezuela, 244 pp.

Etchecopar, A., Vasseur, G., Daignieres, M., 1981. An inverse problem in microtectonics for the determination of stress tensors from fault striation analysis. Journal of Structural Geology 3, 51–65.

Fanti, O., Frontado, L., Vecchio, A., 1980. Tectónica y sismicidad del área de Caracas y sus alrededores. Undergraduate thesis. Universidad Central de Venezuela, 132 pp.

Fleischmann, K., Nemcok, M., 1991. Paleostress inversion of fault-slip data using the shear stress solution of Means (1989). Tectonophysics 196, 195–202.

Freymueller, J.T., Kellogg, J.N., Vega, V., 1993. Plate motions in the north Andean region. Journal of Geophysical Research 98, 21853–21863.

Funvisis, 1984. Estudios de Riesgo Sísmico, Ferrocarril Caracas-La Guaira. Unpublished Funvisis' report for Ferrocar. 2 Vol. + 3 appendices.

Funvisis et al., 1997. Evaluación preliminar del sismo de Cariaco del 09 de Julio de 1997, Estado Sucre, Venezuela (versión revisada). Funvisis. 123 pp + 5 appendices.

Gallardo, C., 1985. Esquisse sismotectonique de la region centro-occidentale du Venezuela et sa relation avec la geodynamique des Caraïbes. PhD thesis, Université de Montpellier II (U.S.T.L.), 276 pp.

Giraldo, C., 1985a. Neotectónica y sismotectónica de la región de El Tocuyo-San Felipe (Venezuela centro-occidental). Proceedings VI Congreso Geológico Venezolano, Caracas, vol. 4, pp. 2415–2451.

Giraldo, C., 1985b. Néotectonique et sismotectonique de la région d'El Tocuyo-San Felipe (Vénézuéla centro-occidental). PhD thesis, Université de Montpellier II, 130 pp.

Giraldo, C., Beltrán, C., 1988. Evaluación del campo de esfuerzos durante el Cuaternario en la región nororiental de Venezuela (Proyecto CONICIT S1-1161). Unpublished Funvisis' report for CONICIT, 68 pp.

Hancock, P., Barka, A., 1987. Kinematic indicators on active normal faults in western Turkey. Journal of Structural Geology 9, 573–584.

Hernández, J., Rojas, E., 2002. Estudio tectono-estratigráfico del borde meridional de la cuenca de Barlovento, estado Miranda. Implicaciones neotectónicas. Unpublished undergraduate thesis, Universidad Central de Venezuela.

Hess, H., Maxwell, J., 1953. Caribbean research project. Bulletin of the Geological Society of America 64 (1), 1–6.

Jácome, M.I., 1994. Interpretación geológica, sísmica y gravimétrica de un perfil transandino. Undergraduate thesis, Universidad Simón Bolívar, Caracas, Venezuela, 68 pp.

Jaimes, M., Pérez, O., Garciacaro, E., 1998. Subducción de la Placa del Caribe bajo la Sudamericana en el Noroeste de Venezuela: evidencias sismológicas. Proceedings IX Congreso Venezolano de Geofísica, CD-Rom; paper no. 39.

Jordan, T., 1975. The present-day motions of the Caribbean plate. Journal of Geophysical Research 80, 4433–4439.

Kafka, A., Weidner, D., 1981. Earthquake focal mechanisms and tectonic processes along the Southern boundary of the Caribbean Plate. Journal of Geophysical Research; 86 (B4), 2877–2888.

Kaniuth, K., Drewes, H., Stuber, K., Temel, H., Hernández, J.N., Hoyer, M., Wildermann, E., Kahle, H.G., Geiger, A., 1999.

Position changes due to recent crustal deformations along the Caribbean–South American plate boundary derived from CASA GPS project. General Assembly of the International Union of Geodesy and Geophysics (IUGG), Birmingham, U.K. Poster at Symposium G1 of International Association of Geodesy.

Kellogg, J., Bonini, N., 1982. Subduction of the Caribbean Plate and Basament Uplifts in the overriding South-American Plate. Tectonics 1 (3), 251–276.

Kellogg, J., Vega, V., 1995. Tectonic development of Panama, Costa Rica, and the Colombian Andes: Constraints from Global Positioning System geodetic studies and gravity. Special Paper-Geological Society of America 295, 75–90.

Kozuch, M., 1995. Earthquake Hazard Analysis of Venezuela using site-specific attenuation. PhD thesis, University of Colorado, 154 pp.

Laffaille, J., 1981. Mecanismos focales de algunos eventos sísmicos ocurridos en el Occidente de Venezuela. Undergraduate thesis, Universidad de Los Andes, Mérida, 142 pp.

Loyo, B., 1986. Estudio Tecto-estratigráfico de la Cuenca del Tuy, Edo. Miranda, Venezuela. Undergraduate thesis, Universidad Central de Venezuela, 179 pp.

Lozano, I., 1984. Microsismicidad en los alrededores de Gavidia, Edo. Mérida. Undergraduate thesis in Physics, Universidad de Los Andes, Mérida, 137 pp.

Malavé, G., 1992. Inversión de ondas de volumen de algunos sismos importantes del noroccidente de Venezuela: relación con la tectónica regional. Master thesis, Instituto de Geofísica, UNAM, México, 93 pp.

Malavé, G., 1997. Sismotectónica del Occidente de Venezuela. PhD thesis, Instituto de Geofísica, UNAM, México, 224 pp.

Malavé, G., Súarez, G., 1995. Intermediate-depth seismicity in northern Colombia and western Venezuela and its relationship to Caribbean plate subduction. Tectonics 14 (3), 617–628.

Malfait, B., Dinkelman, M., 1972. Circum-Caribbean tectonic and igneous activity and the evolution of the Caribbean plate. Geological Society of America Bulletin 83 (2), 251–272.

Marín, L., 1982. Mecanismo focal de algunos eventos sísmicos ocurridos en Venezuela. Undergraduate thesis, Facultad de Ingeniería, Escuela de Ingeniería Geodésica, Universidad del Zulia, Maracaibo.

Mathieu, X., 1989. La Serrania de Trujillo-Ziruma aux confins du Bassin de Maracaibo, de la Sierra de Falcon et de la Chaine Caraïbe. PhD thesis, Université de Brest. 266 pp + appendices.

Mattauer, M., 1973. Les déformations des matériaux de l'ecorce terrestre. Hermann, Paris.

Mendoza, J., 1989. Reporte especial sobre los sismos del Táchira ocurridos en Enero-Febrero de 1989. Unpublished Funvisis' report.

Minster, J., Jordan, T., 1978. Present-day plate motions. Journal of Geophysical Research 83, 5331–5354.

Mocquet, A., 1984. Phases de déformation plio-cuaternaire liées au fonctionnement d'une faille transformante émergée: La faille d'El Pilar (Vénézuéla). Memoir D.E.A., Université de Rennes, 35 pp.

Molnar, P., Sykes, L., 1969. Tectonics of the Caribbean and Middle America Regions from focal mechanisms and Seismicity. Geological Society of America Bulletin 80, 1639–1684.

Muñoz, M., 2002. Evaluación geomecánica para la estimación de los esfuerzos (dirección-magnitud) in-situ del Domo de Santa Rosa, en las formaciones San Juan y San Antonio (Cretácico), Merecure (Oligoceno) y Oficina (Mioceno), area Mayor de Anaco (AMA), edo. Anzoátegui, en el desarrollo de la perforación. Undergraduate thesis, Universidad Central de Venezuela. 134 p.

Palme, C., Choy, J., Morandi, M., 2001. Mecanismos focales sísmicos y esfuerzos tectónicos en la región norte de los Andes merideños, Venezuela. Interciencia 26 (5), 201–209.

Pennington, W., 1981. Subduction of the Eastern Panama Basin and Seismotectonics of Northwestern South America. Journal of Geophysical Research 86 (B11), 10.753–10.770.

Pérez, O., 1998. Seismological Report on the Mw 6.8 Strong Shock of 9 July 1997 in Cariaco, northeastern Venezuela. Short Notes, Bulletin of the Seismological Society of America 88 (3), 874–879.

Pérez, O., Aggarwal, Y., 1981. Present-day tectonics of southeastern Caribbean and northeastern Venezuela. Journal of Geophysical Research 86, 10791–10805.

Pérez, O., Jaimes, M., Garciacaro, E., 1997a. Microseismicity evidence for subduction of the Caribbean plate beneath the South American plate in northwestern Venezuela. Journal of Geophysical Research 102 (B8), 17.875–17.882.

Pérez, O., Sanz, C., Lagos, G., 1997b. Microseismicity, tectonics and seismic potential in southern Caribbean and northern Venezuela. Journal of Seismology 1, 15–28.

Pérez, O., Bilham, R., Bendick, R., Hernández, N., Hoyer, M., Velandia, J., Moncayo, C., Kozuch, M., 2001. Velocidad relativa entre las placas del Caribe y Sudamérica a partir de observaciones dentro del sistema de posicionamiento global (GPS) en el norte de Venezuela. Interciencia 26 (2), 69–74.

Petit, J.-P., Proust, F., Tapponnier, P., 1983. Critères de sens de mouvement sur les miroirs de failles en roches non calcaires. Bulletin de la Société Géologique de France XXV, 589–608.

Phan-Trong, T., 1993. An inverse problem for the determination of the stress tensor from polyphased fault sets and earthquake focal mechanisms. Tectonophysics 224, 393–411.

Pindell, J., Dewey, J., 1982. Permo-Triassic reconstruction of western Pangea and the evolution of the Gulf of Mexico/ Caribbean region. Tectonics 1 (2), 179–211.

Proust, F., Petit, J-P., Tapponnier, P., 1977. L'accident du Tizi n'Test et le rôle des décrochements dans la tectonique du Haut Atlas occidental (Maroc). Bulletin de la Société Géologique de France XIX, 541–551.

Ramos, C., Mendoza, J., 1991. Actividad Sísmica en la costa nororiental del estado Falcón entre los días 26-04-89 y 02-06-89. Unpublished Funvisis' report, 28 pp.

Ramos, C., Mendoza, J., 1993. Actividad Sísmica al sur de la isla La Tortuga entre los días 18 de marzo y 13 de Abril de 1990. Boletín-Instituto de Materiales y Modelos Estructurales, IMME-UCV 80, 69–86.

Rial, J., 1978. The Caracas, Venezuela, earthquake of July 1967: a multiple-source event. Journal of Geophysical Research 83 (B11), 5.405–5.414.

Ritz, J.-F., 1991. Évolution du champ de contraintes dans Les Alpes du sud depuis la fin de l'Oligocène. Implications sismotectoniques. PhD thesis, Université de Montpellier II.

Rod, E., 1956a. Earthquakes of Venezuela related to strike slip faults? Bulletin of the American Association of Petroleum Geologists 40, 2509–2512.

Rod, E., 1956b. Strike-slip faults of northern Venezuela. Bulletin of the American Association of Petroleum Geologists 40 (3), 457–476.

Rodríguez, M., 1995. Estudio del enjambre sísmico ocurrido en el estado Táchira en el año 1994. Undergraduate thesis, Escuela de Ciencias, Departamento de Física, Universidad de Oriente, 57 pp.

Romero, G., 1993. Estudio y Determinación de Características de Fuentes Sísmicas en Venezuela por Medio del Análisis Espectral de Ondas Corpóreas. Master thesis, Universidad Central de Venezuela. Caracas.

Romero, G., 1994. Recopilación y base de datos de mecanismos focales en Venezuela y zonas adyacentes. Unpublished Funvisis' report, 29 pp.

Russo, R., 1999. Dynamics and deep structure of the southeastern Caribbean–South America Plate Boundary Zone: relationship to shallow seismicity. AGU Spring Meeting, Boston, U.S.A., pp. S228. abstract.

Russo, R., Speed, R., 1992. Oblique collision and tectonic wedging of the South American continent and Caribbean terranes. Geology 20, 447–450.

Russo, R., Okal, E., Rowley, K., 1992. Historical seismicity of the Southeastern Caribbean and tectonic implications. Pure and Applied Geophysics 139 (1), 87–120.

Saleh, J., Weber, J., Balkaransingh, S., Dixon, T., Ambeh, W., Leong, T., Charles, F., Wdowinski, S., Webb, F., under review. Neotectonics and seismic risk in Trinidad, West Indies, from historic triangulation (1901–1903) and GPS (1994–1999) Geodesy. Journal of Geophysical Research.

Sánchez, M., Vásquez, A., Van Alstine, D., Butterworth, J., García, J., Carmona, R., Poquioma, W., Ramones, M., 1999. Application of geomechanics in the development of the naturally fractured carbonates of the Mara Oeste field, Venezuela. 1999 SPE Latin American and Caribbean Petroleum Engineering Conference, Caracas, Venezuela, SPE 54008.

Schubert, C., 1979. El Pilar fault zone, northeastern Venezuela: brief review. Tectonophysics 52, 447–455.

Schubert, C., 1980a. Morfología neotectónica de una falla rumbo-deslizante e informe preliminar sobre la falla de Boconó, Andes merideños. Acta Científica Venezolana 31, 98–111.

Schubert, C., 1980b. Late Cenozoic pull-apart basins, Boconó fault zone, Venezuelan Andes. Journal of Structural Geology 2 (4), 463–468.

Schubert, C., 1982. Neotectonics of the Boconó fault, western Venezuela. Tectonophysics 85, 205–220.

Schubert, C., 1984. Basin formation along Boconó–Morón–El Pilar fault system, Venezuela. Journal of Geophysical Research 89, 5711–5718.

Singer, A., Audemard, F.A., 1997. Aportes de Funvisis al desarrollo de la geología de fallas activas y de la paleosismología para los estudios de amenaza y riesgo sísmico. Publucación Especial Academia de las Ciencias Naturales, Matemáticas y Físicas 33, 25–38.

Slemmons, D., 1977. Faults and earthquake magnitudes. Miscellaneous paper S-73-1, U.S. Army Engineer Waterways Experiment Station, Vicksburg.

Sobiesiak, M., Alvarado, L., Vásquez, R., 2002. Sisimicidad reciente del Oriente de Venezuela. XI Congreso Venezolano de Geofísica, 4pp. (CD-Rom format).

Soulas, J-P., 1986. Neotectónica y tectónica activa en Venezuela y regiones vecinas. Proceedings VI Congreso Geológico Venezolano, Caracas, 1985, vol. 10, pp. 6639–6656.

Soulas, J.-P., Giraldo, C., Bonnot, D., Lugo, M., 1987. Actividad cuaternaria y características sismogénicas del sistema de fallas Oca–Ancón y de las fallas de Lagarto, Urumaco, Río Seco y Pedregal. Afinamiento de las características sismogénicas de las fallas de Mene Grande y Valera. (Proyecto COLM). Unpublished Funvisis' report for Intevep, 69 pp.

Stephan, J.-F., 1982. Evolution géodinamique du domaine Caraïbe, Andes et chaine Caraibe sur la transversale de Barquisimeto (Vénézuéla). PhD thesis, Paris, 512 pp.

Suárez, G., Nabelek, J., 1990. The 1967 Caracas Earthquake: fault geometry, direction of rupture propagation and seismotectonic implications. Journal of Geophysical Research 95 (B11), 17459–17474.

Sykes, L., McCann, W., Kafka, A., 1982. Motion of Caribbean Plate during last 7 million years and implications for earlier Cenozoic movements. Journal of Geophysical Research 87 (B13), 10656–10676.

Tjia, H., 1971. Fault movement, reoriented stress field and subsidiary structures. Pacific Geology 5, 49–70.

Tovar, E., 1989. Recopilación y obtención de mecanismos focales en Venezuela. Unpublished Funvisis' report.

Trenkamp, R., Kellogg, J., Freymueller, J., Mora, H., 2002. Wide plate margin deformation, southern Central America and northwestern South America, CASA GPS observations. Journal of South American Earth Sciences 15, 157–171.

Valera, M., 1995. Estudio de la tormenta sísmica ocurrida en el estado Lara en los meses Agosto–Septiembre de 1991. Undergraduate thesis, Escuela de Ciencias, Departamento de Física, Universidad de Oriente, 66 pp.

Van der Hilst, R., 1990. Tomography with P, PP, and pP delay-time data and the three-dimensional mantle structure below the Caribbean region. PhD thesis, University of Utrecht, Netherlands, Geologica Ultraiectina 67, 250 pp.

Vedder, J., Wallace, R., 1970. Map showing recently active breaks along the San Andreas and related faults between Cholame Valley and Tejon Pass, California. U. S. Geological Survey Miscellaneous Geologic Investigations Map I-574, scale 1:24,000.

Wadge, G., Burke, K., 1983. Neogene Caribbean plate rotation and associated Central American tectonic evolution. Tectonics 2 (6), 633–643.

Weber, J., Dixon, T., DeMets, C., Ambeh, W., Jansma, P., Mattioli, G., Saleh, J., Sella, G., Bilham, R., Pérez, O., 2001a. GPS estimate of relative motion between the Caribbean and South American plates, and geologic implications for Trinidad and Venezuela. Geology 29 (1), 75–78.

Weber, J., Ferrill, D., Roden-Tice, M., 2001b. Calcite and quartz microstructural geothermometry of low-grade metasedimentary rocks, Northern Range, Trinidad. Journal of Structural Geology 23, 93–112.

Wesson, R., Helley, E., Lajoie, K., Wentworth, C., 1975. Faults and future earthquakes U.S. Geological Survey Professional Paper P941A.

Wilcox, R., Harding, T., Seely, D., 1973. Basic wrench tectonics. Bulletin of the American Association of Petroleum Geologists 57, 74–96.

Willson, S.M., Last, N.C., Zoback, M.D., Moos, D., 1999. Drilling in South America: a wellbore stability approach for complex geologic conditions. 1999 SPE Latin American and Caribbean Petroleum Engineering Conference, Caracas, Venezuela, SPE 53940.

Wozniak, J., Wozniak, M., 1979. Geología de la región de Cabure Estado Falcón. Unpublished Ministerio de Energía y Minas' report, 64 pp + appendices.

Ysaccis, R., Cabrera, E., Del Castillo, H., 2000. El sistema petrolífero de la Blanquilla, costa afuera Venezuela. Proceedings VII Congreso Bolivariano Exploración Petrolera en las Cuencas Subandinas, Caracas, pp. 411–425.